Plant Physiology Preview. Published on August 28, 2020, as DOI:10.1104/pp.20.00689

Short title:

Altered auxin response in *tarani/ubp14* mutant

Corresponding author(s) details:

Utpal Nath, Associate Professor, Department of Microbiology and Cell Biology, Indian Institute of Science, Bengaluru, India; phone + 91 (0)80 22932414; fax+ 91 (0)80 23602697

Title: The ubiquitin-specific protease TNI/UBP14 functions in ubiquitin recycling and affects auxin response

All authors names and affiliations:

Parinita Majumdar[1,*], Premananda Karidas[1,*], Imran Siddiqi[2] and Utpal Nath[1,#]

[1]Department of Microbiology and Cell Biology, Indian Institute of Science, Bangalore 560 012, India

[2]Centre for Cellular and Molecular Biology, Uppal Road, Hyderabad, 500 007, India

[*] These two authors contributed equally

One-sentence summary:

Arabidopsis TNI/UBP14 destabilizes AUX/IAA repressors and promotes auxin response by ubiquitin recycling.

Author contributions:

PK mapped and cloned *TNI*, performed part of phenotypic analysis, generated *TNI* over-expression line, down-regulation line and *pTNI::GUS* line and analyzed them; PM performed part of phenotypic analysis and all the auxin-related experiments, analyzed the data, made the figures and wrote the first draft of the MS. IS guided PK with intellectual and material inputs in cloning *TNI*. UN contributed in designing experiments, guided the first two authors and finalized the manuscript.

Funding information:

PM and PK were supported by fellowships from Ministry of Human Resource Development, Government of India. UN is thankful to DST-FIST, UGC Centre for Advanced Study and DBT-IISc Partnership Program Phase-II at IISc (sanction No. BT/PR27952/INF/22/212/2018) for the funding and infrastructure support.

Corresponding author email:
utpalnath@iisc.ac.in

ABSTRACT

The ubiquitin-mediated proteasomal pathway regulates diverse cellular processes in plants by rapidly degrading target proteins, including the repressors of hormone signaling. Though ubiquitin proteases play key role in this process by cleaving poly-ubiquitin chains to monomers, their function has not been studied in detail by mutational analysis. Here, we show that mutation in *TARANI*/ *UBIQUITIN-SPECIFIC PROTEASE 14*(*TNI*/*UBP14*) leads to reduced auxin response and widespread auxin-related phenotypic defects in *Arabidopsis thaliana*. In a *tni* partial loss-of-function mutant that was originally isolated based on altered leaf-shape, activity of the auxin responsive reporters *DR5::GUS*, *DR5::nYFP* and *IAA2::GUS* was reduced. Genetic interaction studies suggested that *TNI* is involved in auxin signaling and acts alongside*TIR1*, *ARF7*, and *AUX1*. Map-based cloning identified *TNI* as *UBIQUITIN SPECIFIC PROTEASE14*. Inefficient splicing of the mutant *TNI* transcript resulted in the formation of an inactive UBP14 protein, which led to the accumulation of poly-ubiquitin chains and excess poly-ubiquitinated proteins in the mutant. In addition to reduced auxin response, increased DII:VENUS, IAA18:GUS, and HS::AXR3-NT:GUS level was also observed in *tni*, perhaps due to inefficient poly-ubiquitin hydrolysis and proteasome-mediated degradation. Together, our study identifies a function for TNI/UBP14 in auxin response through ubiquitin recycling.

INTRODUCTION

In plants, response pathways of several major phytohormones rely on 26S proteasome-mediated protein degradation. For example, the negative regulators of auxin, gibberellic acid (GA), and jasmonic acid (JA) signaling pathways, such as AUX/IAA, DELLA, and JASMONATE-ZIM DOMAIN (JAZ), respectively, undergo poly-ubiquitination and are subsequently degraded by the 26S proteasome, resulting in a change in gene expression (Daviere and Archard 2013; Gray et al., 2001; Ruegger et al., 1998; Wang and Deng, 2011). The poly-ubiquitin chains generated upon target protein degradation are hydrolysed into mono-ubiquitin by a group of processingenzymes known as de-ubiquitinases (DUBs) (Callis, 2014;Yan et al., 2000; Majumdar and Nath, 2020). These proteases also hydrolyse ubiquitin poly-proteins linked head-to-tail by an α-peptide bond and ubiquitin-ribosomal extension proteins into mono-ubiquitin (Callis, 2014). Thus, DUBs are implicated in ubiquitin recycling

to accomplish diverse cellular function. Domain organization along with the catalytic residues categorizes the DUBs into five families: UBIQUITIN SPECIFIC PROTEASES (UBPs), UBIQUITIN C-TERMINAL HYDROLASES, OVARIAN TUMOR PROTEASES, MACHADO–JOSEPH DOMAIN PROTEASES, and JAB1/MPN/MOV34 proteases (Yan et al., 2000; Isono and Nagel, 2014; Majumdar and Nath, 2020). Among these, UBPs comprise the largest family with 27 members in Arabidopsis (Yan et al., 2000). The T-DNA knock-out lines *ubp14* and *ubp19* show embryonic lethality whereas *ubp15* has narrow and serrated leaves (Liu et al., 2008). Single loss-of-function mutants of the remaining UBPs do not exhibit discernible phenotypic alteration, suggesting genetic redundancy (Liu et al., 2008). However, higher-order mutants exhibit defects in cell cycle progression, endoduplication, gametogenesis, meristem maintenance, and flowering time control (Xu et al., 2016, An et al., 2018; Liu et al., 2008). Most of these UBPs show *in vitro* de-ubiquitination activity against α-linked or iso-linked poly-ubiquitin chains and ribosomal extension proteins (Isono and Nagel, 2014; Majumdar and Nath, 2020).

Among the three phytohormones mentioned above, auxin is a key member that regulates a plethora of growth and developmental programs, including embryogenesis, organ morphogenesis, venation pattern, root development, and gravitropism (Hobbie et al, 2000; Swarup et al., 2005; ten Hove et al., 2015). Studies over the past few decades have characterized the auxin signal transduction pathway, which comprises the TRANSPORT INHIBITOR RECEPTOR1 (TIR1) auxin receptor, AUXIN/INDOLE-3-ACETIC ACID (AUX/IAA) inhibitor proteins, and AUXIN RESPONSE FACTOR (ARF) transcription factors (Ruegger et al., 1998; Reed, 2001). Several genetic and biochemical studies have emphasized the importance of auxin-dependent degradation of AUX/IAAs by $SCF^{TIR1/AFB}$ via the 26S proteasome-mediated degradation pathway for maintaining normal auxin response in Arabidopsis (Gray et al, 2001; Leyser, 2018). Hence, the auxin level of a given cell is translated into a response by activating a set of ARFs throughtheir release from AUX/IAA repression. Gain-of-function mutations in the degron motif of AUX/IAAs enhance their stability, resulting in auxin-related defects in embryogenesis, vein patterns, lateral root formation, and apical dominance. These mutants include *axr3-1*, *slr*, *shy2-2*, *crane-1*/*iaa18-1*,and *iaa28-1* (Fukaki et al., 2002; Leyser et al., 1996; Ploense et al., 2009; Tian and Reed, 1999; Uehara et al., 2008). Single loss-of-function mutants of *AUX/IAAs* do not exhibit visible phenotypic alterations, reflecting genetic redundancy (Okushima et al., 2005).

Perturbation in the components of the 26S proteasome pathway is expected to adversely affect the auxin, GA, and JA pathways since their response is triggered by the degradation of their repressors. However, the functions of only a handful of these components have been analyzed by mutational studies. We previously reported the isolation and characterization of an Arabidopsis mutant named *tarani* (*tni*) with pleiotropic phenotypic defects including altered leaf shape (Karidas Premananda, PhD Thesis, 2014; Karidas et al., 2015). Here, we have identified TNI as UBP14 that is involved in ubiquitin recycling. Each of the null alleles of *UBP14* reported earlier is embryonic lethal, rendering further studies of this gene in post-embryonic development a difficult task (Doellinget al., 2001; Tzafrir et al., 2002). However, the hypomorphic *tni* allele allows us to study the function of UBP14 in post-embryonic development. The only other reported allele of *UBP14* with post-embryonic viability is *da3-1*, which has defective nuclear ploidy and organ growth (Xu et al., 2016). By carrying out detailed phenotypic analysis of *tni* seedlings, we found that TNI/UBP14 is required for optimal auxin response in Arabidopsis. Homozygous *tni* plants showed diverse phenotypic aberrations including defective embryo pattern, tricotyledonous and rootless seedlings, altered root gravitropism, and fewer lateral roots. These defects are also found in mutants with perturbed auxin response. Ubiquitin recycling and turn-over of several AUX/IAAs were perturbed in *tni* seedlings. Together, our study suggests that TNI/UBP14 maintains a balance between poly-ubiquitin and mono-ubiquitin, which is necessary for the turn-over of auxinsignaling repressors through the 26S proteasome and thus required for normal auxin response.

RESULTS

Altered auxin-related phenotype in *tni*

The *tarani* (*tni*) mutant with altered leaf shape was originally isolated in a forward genetic screen (Karidas et al., 2015). Detailed characterization of *tni* revealed multiple defects in embryonic and post-embryonic development (Fig. 1). The *tni* embryo exhibited an aberrant early cell division pattern (Fig. 1 A-C). In wild-type, the apical cell of the 1-cell pro-embryo undergoes vertical division to form the 2-cell pro-embryo and the basal cell undergoes a series of anticlinal division to form the suspensor (Boscá et al., 2011). Whereas the apical cell of each of the wild-type embryos studied (n=30) underwent vertical division, a noticeable fraction of *tni* embryos showed horizontal (~21%, n=87) or oblique (~8%, n=87) division (Fig. 1A; Supplemental Fig. S1A and B). Besides, the topmost suspensor cell in ~36% *tni* embryo (n=38) underwent periclinal division, which was never observed in Col-0 (n=30) (Fig. 1B).Such defects are also observed in the auxin-signaling mutant *bodenlos* (*bdl*) and the higher-order polar auxin-transport mutant *pin2pin3pin4pin7* (*pin-formed*) (Hamann et al., 1999; Blilou et al., 2005). Hypophysis, the precursor of root stem cell initials, undergoes asymmetric division during the dermatogen stage of embryogenesis and forms a lens-shaped cell, which is incorporated into the embryo at the globular stage (Scheres et al., 1994). A normal lens-shaped cell was observed in all the Col-0 globular embryos (n=30), whereas ~7% of *tni* embryos (n=95) did not form a proper lens-shaped cell (Fig. 1C). The lack of such formative division, which is necessary for specifying root stem cell initials, is expected to result in rootless seedlings. We observed ~13% rootless seedlings in *tni* (n=407), which was never seen in Col-0 (n=127) (Fig. 1D). Perturbed auxin signaling in the gain-of-function mutant *bdl* and in the loss-of-function mutant *monopteros* (*mp*) also results in rootless seedlings (Hamann et al., 1999; 2002).

The post-embryonic developmental defects in *tni* included tricotyledonous seedlings, reduced complexity in cotyledon venation, defects in root gravitropic response, fewer lateral roots, larger seeds, and an increase in petal number (Fig. 1E-O). We estimated that ~4% of *tni* seedlings (n=306) form three cotyledons (Fig. 1E), which was never observed in Col-0. To address the origin of this phenotype, we examined the transition-state embryos when cotyledon primordia are initiated (ten Hove et al., 2015). Col-0 embryo always formed two cotyledon primordia whereas *tni* embryo occasionally produced three (Fig. 1F). Tricotyledonous phenotype is also observed in the *pin-formed 1*(*pin1*) loss-of-function

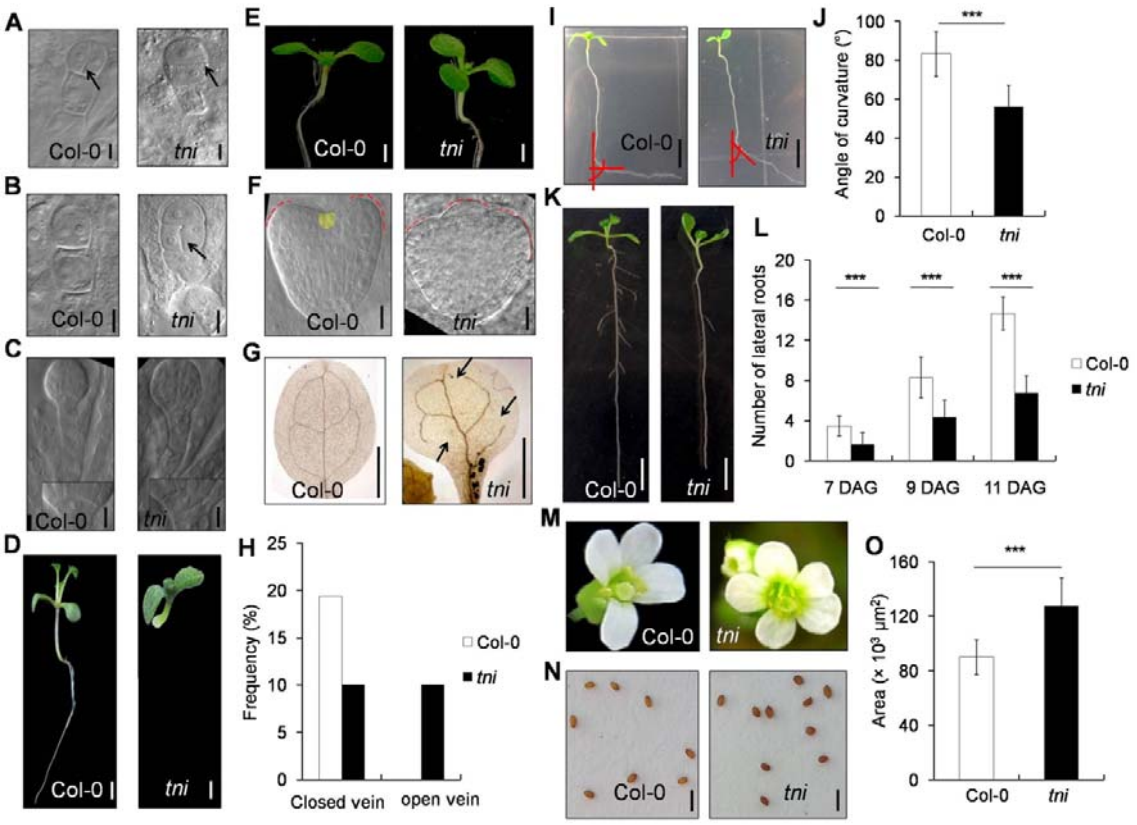

Figure 1. Auxin-related phenotypes in *tni*. **(A)** 2-cell pro-embryo. Arrows highlight vertical (Col-0) or horizontal (*tni*) cell division. **(B)** 1-cell pro-embryo. Arrow indicates periclinal cell division defect in the *tni* basal cell. **(C)** Globular stage embryo. Normal (Col-0) and aberrant (*tni*) lens-shaped cells are magnified in the insets. Scale bar (in **A-C**), 10µm. **(D)** Normal (Col-0) and rootless (*tni*) seedlings. Scale bar, 1mm.The image was digitally extracted to remove the background. **(E)** 7-day-old seedlings with two (Col-0) or three (*tni*) cotyledons. Scale bar, 1mm. The photograph is taken in a black background. **(F)** Heart stage embryo with two (Col-0) or three (*tni*) cotyledon primordial (marked by dotted line). Col-0 meristem is falsely colored in yellow. Scale bar, 10µm. **(G)** Cotyledons from 7-day-old seedlings are cleared to highlight veins. Open venation in *tni* is marked by arrows. Scale bar, 1 mm. **(H)** Percentage of cotyledons (n= 103 in Col-0 and 90 in *tni*) showing closed or open veins. **(I)** Effect of gravistimulation on primary roots of 7-day-old seedlings. Angles of root bending are indicated by red lines. Scale bar, 5 mm. **(J)** Average angle of curvature (n= 52 for Col-0 and 43 for *tni*) of primary roots following gravistimulation shown in **(I)**. Error bars represent SD. *** denotes p<0.0001 (unpaired Student's *t*-test was used). **(K)** 11-day-old seedlings. Scale bar, 5 mm. **(L)** Average number of lateral roots (n= 10–13) in seedlings at indicated days after germination (DAG). Error bars represent SD. *** denotes p<0.0001 (unpaired Student's *t*-test). **(M)** Open flowers showing variation in petal number in *tni* mutant. The image was digitally extracted to remove the background. **(N)** Matured seeds. Scale bar, 1 mm. (O) Average seed area (n= 15). Error bars represent SD. *** denotes p<0.0001 (unpaired Student's *t*-test).

mutant with perturbed auxin transport (Krecek et al., 2009). Mature *tni* cotyledons showed fewer complete areoles (closed veins) as opposed to four complete areoles produced by the Col-0 cotyledons (Fig. 1G and H). Nearly 20% of Col-0cotyledons (n=103) showed maximal complexity with four complete areoles and the remaining had <4 areoles with some open vasculature (Fig. 1H and Supplemental Fig. S1C and D) (Sieburth, 1999). By contrast, only ~10% (n=90) of *tni* cotyledons formed four areoles and another ~10% exhibited an open-top vein defect which was never seen in Col-0 (Fig. 1H). Such a venation defect is also observed in the *auxin-resistant mutant6* (*axr6*) mutant (Hobbie et al., 2000).

The *tni* mutant exhibited defects in the sub-aerial organs as well (Fig. 1I-L). Primary roots in *tni* seedlings showed defects in gravitropic response (Fig. 1I). Col-0 primary roots responded to gravistimulation by bending towards gravity at an average angle of 83.1° ± 11.50 (n=52) (Fig. 1J). By contrast, the *tni* roots bent only by 56.1° ± 11.0 (n=43) under similar experimental conditions, indicating reduced gravitropic response. The *tni* seedlings also produced fewer lateral roots (Fig. 1K and L). In Col-0 seedlings, the number of emerged lateral roots steadily increased from 7 to 11 days after germination (DAG) (Fig. 1L). Though a similar trend was observed in the *tni* seedlings, the number remained ~50% lower at all the growth stages measured. Fewer lateral roots have been reported in mutants with perturbed auxin transport and signaling such as *tir1-1*, *auxin1-7* (*aux1-7*), and *arf7-1* (Ruegger et al., 1998; Marchant et al, 2002; Okushima et al., 2007).

The *tn i*mutant also showed an altered floral phenotype. Whereas all Col-0 flowers (n=142) formed four petals, the petal number in ~58% of *tni* flowers (n=140) increased to 5–6 (Fig. 1M). This phenotype is similar to the weaker allele of polar auxin-transport mutant *pin1-5* (Yamaguchi et al., 2014).In addition, *tni* plants produced bigger seeds with a ~30% increase in seed area compared to wild-type (Fig. 1N and O). Bigger seeds are seen in the mutant of *ARF2*, a negative regulator of cell division and expansion in Arabidopsis (Schruff et al., 2005).

Reduced auxin response in *tni*

The altered phenotype in *tni* described above, also seen in several auxin-pathway mutants (Swarup et al., 2005; Marchant et al., 2002; Ruegger et al., 1998, Bennett et al., 1995), suggests a possible involvement of *TNI* in the auxin pathway. Therefore, we compared auxin response in Col-0 and *tni* seedlings using the auxin-responsive *DR5::GUS*, *DR5::nYFP*, and *IAA2::GUS* reporter lines (Ulmosovet al., 1997; Mähönen et al., 2015; Marchant et al., 2002). GUS assay of 3-day-old *DR5::GUS* seedlings showed strong β-glucuronidase activity throughout the cotyledon margin with the highest signal at the tip, indicative of auxin maxima (Mattsson et al., 2003; Sabatini et al., 1999) (Fig. 2A). However, no distinct auxin maxima were detected in the *DR5::GUS tni* cotyledons, which exhibited an overall reduction in GUS signal except for at the margin. A similar reduction in auxin maxima was also observed at the tip of emerging leaves, primary roots, and lateral roots of *DR5::GUS tni* seedlings (Fig. 2B-D). Comparison of the fluorescence signal in *DR5::nYFP* Col-0 and *DR5::nYFP tni* also revealed reduced auxin maxima at the cotyledon tips (Fig. 2E) and root

189 tips (Fig. 2F),whereas the nYFP signal was increased in the *tni* columella cells, which

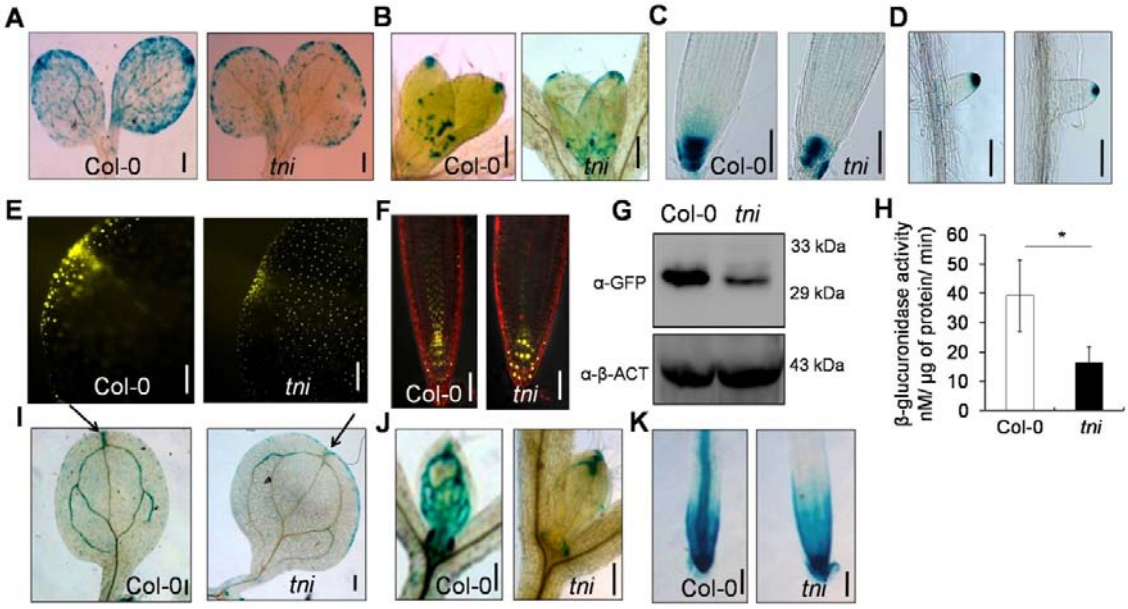

Figure 2. Auxin response in *tni*. (A-D) DR5::GUS activity in the cotyledons (**A**), first leaf pair **(B)**, primary root tips **(C),** and lateral root tips **(D)** of 3-**(A)** and 7-day-old (**B-D**) *DR5::GUS* (Col-0) and *DR5::GUS tni* (*tni*) seedlings. Scale bar, 200µm (**A**, **B**) and 100µm (**C**, **D**). **(E** and **F)** DR5::nYFP signal at the tips of cotyledons of 5-day-old seedlings (**E**) and primary roots (**F**) of 7–8-day-old *DR5::nYFP* (Col-0) and *DR5::nYFP tni* (*tni*) seedlings. Scale bar, 50µm (**E**, **F**). Root samples were stained with propidium iodide in (**F**). **(G)** Western blots of the total proteins from 7-day-old *DR5::nYFP* (Col-0) and *DR5::nYFP tni* (*tni*) seedlings. α-β-ACTIN (α-β-ACT) was used as a control. **(H)** β-glucuronidase activity estimated in total extracts of *DR5::GUS* (Col-0) and *DR5::nYFP tni* (*tni*) seedlings. Averages of three biological replicates are shown. Error bars represent SD. * indicates p=0.0406 (unpaired Student's *t*-test). **(I-K)** IAA2::GUS activity in the cotyledons (**I**), first leaf pairs **(J)** and primary roots **(K)** of 7-day-old *IAA2::GUS* (Col-0) and *IAA2::GUS tni* (*tni*) seedlings. Arrows in (**I**) indicate IAA2::GUS activity at cotyledon tips. Scale bar, 200µm (**I**, **J**) and 100µm **(K)**.

190 appeared to have bigger nuclei (Fig. 2F). Quantitative analysis of DR5 activity by Western
191 blot analysis using anti-GFP antibody showed reduced DR5::nYFP signal in the *DR5::nYFP*
192 *tni* seedlings compared to *DR5::nYFP* (Fig. 2G). Similarly, the β-glucuronidase activity was
193 reduced to nearly half in *DR5::GUS tni* seedlings compared to *DR5::GUS* (Fig. 2H). These
194 results suggest that auxin response is reduced in the *tni* mutant.

195 *IAA2* is an immediate auxin-responsive gene whose induction depends on the endogenous
196 auxin level. IAA2::GUS signal was detected primarily in the vasculature of Col-0 cotyledons,
197 leaves, and primary roots, and in the root meristematic region (Fig. 2I-K), which is consistent
198 with previous reports (Marchant et al, 2002). By contrast, vascular *IAA2::GUS* activity in *tni*
199 was reduced in each of these organs with expression limited only to their tips. In addition,
200 ectopic expression was observed in the *tni* cotyledon margin(Fig. 2I).

The histochemical analysis of DR5::GUS and IAA2::GUS described above, together with the DR5::nYFP expression data, suggests that auxin response is reduced in *tni*. The dataset of an earlier microarray experiments carried out on young *tni* leaves (Karidas et al., 2015) identified 29 auxin-related genes that were differentially expressed by>2-fold (16 down-regulated and 13 up-regulated) in *tni* compared to wild-type (Supplemental Fig. S2A). These genes are predicted to regulate auxin biosynthesis, transport, or signaling. Many of these transcripts are also altered in seedlings externally treated with indole-3-acetic acid (IAA) (Supplemental Fig. S2B). Taken together, it appears that TNI is required to maintain normal auxin response in Arabidopsis.

Altered sensitivity of *tni* to external auxin manipulation

Altered auxin response in *tni* could be due to perturbed auxin level or signaling. To test this, we compared the sensitivity of Col-0 and *tni* seedlings towards exogenous administration of the synthetic auxin 1-naphthaleneacetic acid (NAA). Since auxin is known to stimulate lateral root formation in a dose-dependent manner (Ivanchenko et al., 2010), we used the number of lateral roots as a read-out of auxin sensitivity. In Col-0, the number of lateral roots progressively increased with increased concentrations of NAA up to 100 nM, followed by a decrease with a further increase in NAA concentration (Fig. 3A and B), thus forming a characteristic bell-shaped auxin-response curve (Ivanchenko et al., 2010). Though a similar trend was observed for *tni* roots, the peak response in *tni* was achieved at a NAA concentration (200 nM) that was twice that required for Col-0 (Fig. 3B), consistent with its reduced auxin-response phenotypes (Fig. 2). Conversely, *tni* showed increased sensitivity towards the polar auxin transport inhibitor N-1-naphthylphthalamic acid (NPA), which blocks lateral root initiation by reducing the IAA level at the basal root meristem (Casimiro et al., 2001). The total number of lateral roots in Col-0 remained unaltered up to400 nM NPA, beyond which the value declined to ~20% at 1 μM concentration (Fig. 3C and D). In *tni*, the lateral root number reduced to <40% at 400 nM NPA and to nearly zero at 1 μM concentration. Taken together, these results suggest a reduced endogenous auxin response in *tni* roots.

Genetic interaction between *tni* and mutants with auxin-related growth defects

To assess the genetic link between *TNI* and the auxin pathway, we crossed *tni* with mutants defective in auxin signaling and transport, such as *arf7-1*, *tir1-1*, and *aux1-7*, and studied the phenotypes of the double homozygous lines. *ARF7* and *ARF19* redundantly promote lateral

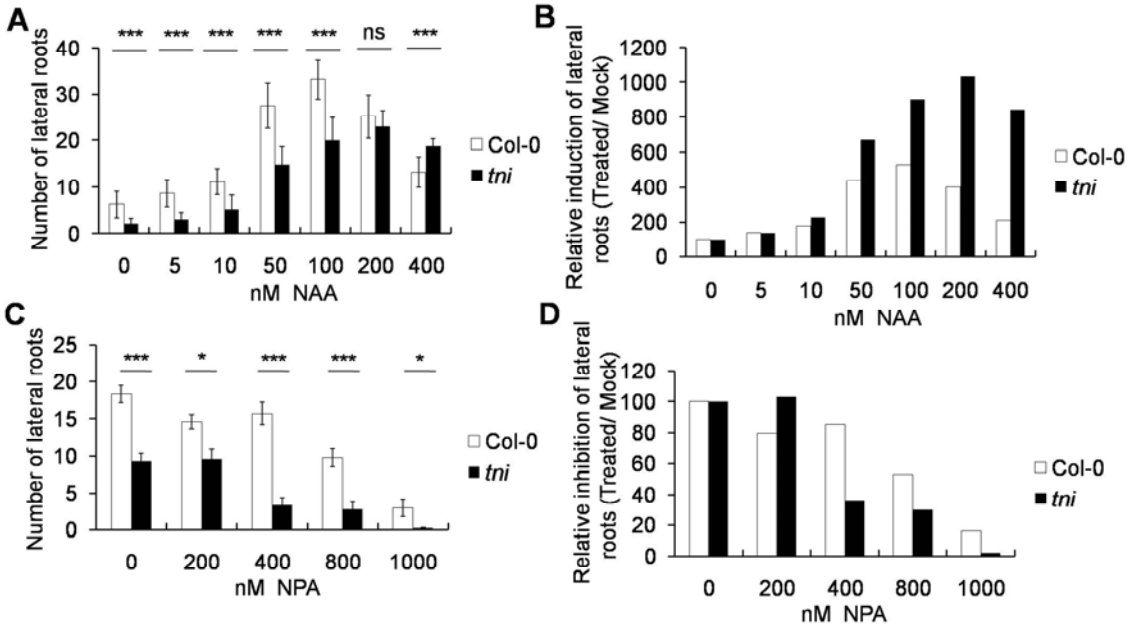

Figure 3. Auxin sensitivity of *tni* mutant. (**A and B**) Average number of lateral roots of 7-day-old seedlings grown in the presence of 1-naphthaleneacetic acid (NAA) (**A**) and their relative increases (**B**). Error bars represent SD. Statistical analysis was done using unpaired Student's *t*-test. *** denotes p≤0.0001. ns, not significant. **(C and D)** Average number of lateral roots in 9-day-old seedlings treated with N-1-naphthylphthalamic acid (NPA) and their relative decreases (**D**). For (**A** and **C**), n= 12–15; error bars represent SD; *** and * denote p≤0.0001 and <0.006, respectively (unpaired Student's *t*-test); ns, not significant.

root formation and the *arf7-1*single mutant produces fewer lateral roots (Okushima et al., 2005, 2007). Since *arf19-1* is a weak allele and *arf7-1 arf19-1* double mutant totally lacks lateral roots, we studied the genetic interaction of *tni* with *arf7-1*. Lateral root formation was severely reduced in the *arf7-1 tni* double mutant compared to the parental lines (Fig. 4A). The auxin-receptor mutant *tir1-1* also forms fewer lateral roots than Col-0 (Ruegger et al., 1998), and the number was further reduced in the *tir1-1 tni* double mutant (Fig. 4B). *AUX1* encodes an auxin-influx carrier that promotes lateral root formation by facilitating the distribution of auxin from leaf to root, and *aux1-7* seedlings make fewer lateral roots and lateral root primordia (LRP) (Marchant et al., 2002). Phenotypic analysis showed that the *aux1-7 tni* mutant had fewer lateral roots than either of the parents (Fig. 4C). Since the mutant alleles used in these genetic interaction studies were weak in nature, one interpretation of these results is that *TNI* works in the auxin-response pathway.

TNI encodes UBP14

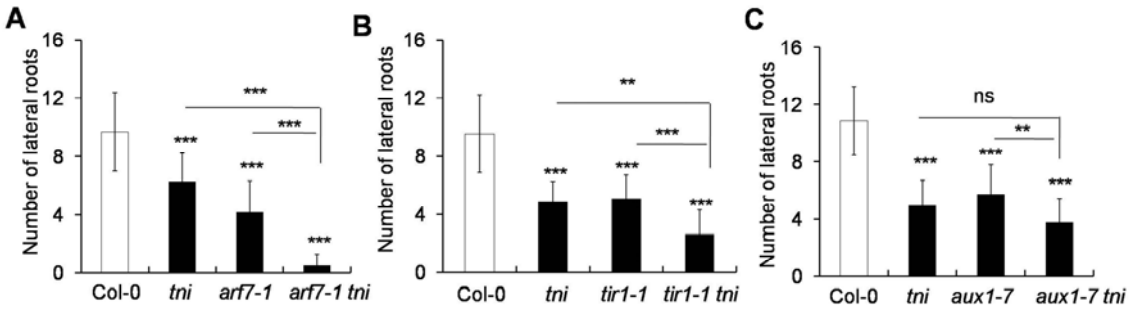

Figure 4. Genetic interaction between *tni* and mutants with auxin-related defects. (A-C) Average number of lateral roots (n= 10–15) of 9-day-old seedlings. Error bars represent SD. *** denotes p<0.0001, ** denotes p= 0.0084 (unpaired Student's *t*-test), ns, not significant.

Using a map-based cloning approach, we delimited the *tni* locus to a 65-kb long genomic region with the help of 927 recombinant mutant plants in a mapping population (see *Methods*). Sequencing of the protein-coding genes within this interval identified an exonic G→A transition in the *At3G20630* locus (Fig. 5A and Supplemental Fig. S3A and B). This mutation mapped at the canonical 3′ splice acceptor site at the junction of the 3rd intron and the 4th exon. *At3G20630*is predicted to encode UBP14, a ZnF de-ubiquitinase protein involved in ubiquitin recycling (Doelling et al., 2001; Xu et al., 2016). Several alleles of *At3G20630* had been previously described (Fig. 5A), most of which show embryonic lethality (Majumdar and Nath, 2020). To further examine *tni* identity, we performed an allelism test with *titan6-4* (*ttn6-4*), a known allele of *UBP14* (Tzafrir et al., 2002). When *tni*/*tni* plants were crossed to *ttn6-4*/+heterozygous plants (which resembled Col-0), 12 out of 42 F_1 individuals produced cup-shaped rosette leaves (Fig. 5B-D), whereas *tni*/+ plants always resembled Col-0 suggesting that *tni* is allelic to *ttn6*. Further, the cup-shaped phenotype of *tni* leaves was partly rescued by over-expressing the wild-type *TNI* transcript; 3 out of 14 hygromycin-resistant transformants recovered and produced flat rosette leaves, though they were rounder than the Col-0 leaves (Fig. 5E). In addition, expressing an artificial microRNA targeting the wild-type *TNI* transcript under the constitutive *RPS5a* promoter in the Col-0 background partially recapitulated the *tni* phenotype (Fig. 5F); 3 out of 25 hygromycin-resistant transformants recovered produced rosette leaves with weak cup-shaped lamina.

The *tni* locus encodes TNI^{intron}, an aberrant UBP14

The wild-type *TNI* locus consists of 20 exons and 19 introns, which is predicted to encode a 88-kDa protein product (Fig. 5A; Supplemental Fig.S3C). If the G→A transition interferes in splicing, the *tni* locus is predicted to produce an additional aberrant transcript (*TNI^{intron}*),

269 whereby 102 nucleotides corresponding to the 3rd intron are retained in frame in the wild-type

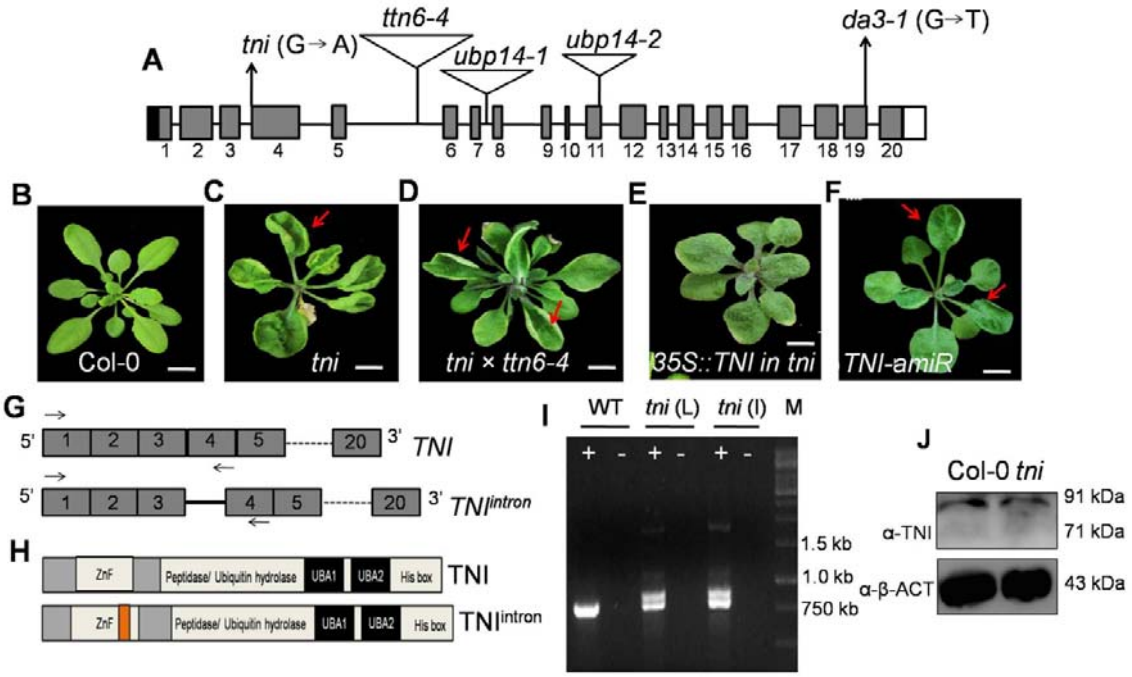

Figure 5. Cloning of *TNI*. (A) A schematic representation of *TNI/UBP14* locus showing 5′ UTR (black box), exons (grey box), introns (black line), and 3′ UTR (white box). Positions of T-DNA insertion in various mutant alleles are shown by inverted triangles. The *G→A* transition at the third intron-exon junction in *tni* allele and *G→T* substitution at the nineteenth exon-intron junction in the *da3-1* allele are indicated. **(B-F)** 30-day-old rosettes of wild-type **(B),** *tni* **(C)**, *tni* x *ttn6-4* (+/-) F_1 plants **(D)**, *tni* plants over-expressing *TNI* transcript **(E)**, and Col-0 plant expressing artificial microRNA (amiR) against *TNI* transcript **(F)**. Red arrows indicate leaf curvature. Scale bar, 0.5 cm.The rosette images in **(B-F)** were digitally extracted to remove the background. **(G)** Schematic representations of the predicted wild-type *TNI* and the mutant TNI^{intron} transcripts. Note the retention of the 3rd intron (solid line) in TNI^{intron}. Arrows indicate the position of the primers used for RT-PCR analysis. Dotted lines indicate continuity of exons. **(H)** Domain architecture of TNI and TNI^{intron} proteins. Orange box indicates a 34 amino acid-residue insertion encoded by the 3rd intron. **(I)** Ethidium bromide-stained agarose gel showing the products of RT-PCR on total RNA from Col-0 (WT), mature *tni* leaves (*tni* L) and *tni* inflorescence (*tni* I). + and - indicate cDNA and RNA as PCR templates. M, DNA marker. **(J)** Western blot of total protein extracted from 7-day-old seedlings using antibody raised against a peptide corresponding to residues 156–174 of TNI. α-β-ACTIN (α-β-ACT) was used as loading control.

270 transcript (Fig. 5G).Whereas RT-PCR analysis with primers flanking the 3rd intron (Fig. 5G)
271 detected a single product of 750 bp in both Col-0 and *tni*, an additional band corresponding to
272 the retention of the 3rd intron was detected in the *tni* samples (Fig. 5I). The intensity of these
273 two bands in *tni* mutant, which corresponded to *TNI* and TNI^{inron} transcripts,seemed
274 comparable, indicating nearly equal abundance of the two transcripts. Transgenic Col-0

plants expressing the *RPS5a::TNI*^{intron} cassette produced cup-shaped leaves in the T_1 generation (Supplemental Fig. S3E); 2 out of 107 independent insertion lines produced all cup-shaped leaves,whereas another 32 lines showed at least one cup-shaped leaf. This genetic evidence suggests an association between retention of the 3rd*TNI* intron and the *tni* phenotype.

Western blot analysis using an antibody generated against a 19-residue polypeptide within the ZnF domain detected a single band in both Col-0 and *tni* seedlings that corresponded to the endogenous TNI (see *Methods*) (Fig. 5J; Supplemental Fig. S3F). This antibody also detected the GST-TNI fusion protein but failed to recognize a truncated TNI that lacked the ZnF domain (Supplemental Fig. S3G and H), suggesting that the antibody is specific to TNI. The *TNI*^{intron} transcript is likely to encode a full-length TNI protein wherein the ZnF domain is disrupted by an insertion of an additional 34 residues (Fig. 5H; Supplemental Fig. S3D). Since both wild-type and mutant transcripts were detected in equal proportion in*tni*(Fig. 5I), it is likely that both TNI (88 kDa) and its mutant variant TNI^{intron} (92 kDa) are translated in *tni* (Fig. 5J), though they cannot be resolved in Western blot analysis due to their similar molecular weights. Indeed, the anti-GST antibody could not distinguish between recombinant GST-TNI and GST-TNI^{intron} in Western blot analysis (Supplemental Fig. S3H).

Cell type-specific TNI activity regulates lateral root formation

UBP14 has been reported to be detected ubiquitously in all tissue types (Doelling et al., 2001; Xu et al., 2016). Consistently, GUS activity was detected throughout the seedlings in all five independent *pTNI::GUS* reporter lines that we generated (Supplemental Fig. S4). In primary roots, more intense GUS signal was detected in discrete pericycle cells that initiate lateral roots (De Smet et al., 2012). Thus, promotion of lateral roots by *TNI* (Fig. 1K and L) could be due to its local expression in roots or due to the systemic effect of auxin response. To test this, we manipulated *TNI* expression in the lateral root initials of transgenic plants and studied its effect on lateral roots. When we expressed an artificial microRNA against *TNI* under the truncated *PLETHORA7* promoter (*pPLT7*) that is active specifically in LRPs (Prasad et al., 2011), lateral root number was reduced by 45–80% in six independent *pPLT7::TNI-amiR* transgenic lines in the T_2 generation Reduced lateral root number was also observed in two homozygous *pPLT7::TNI-amiR* transgenic lines established in the T_3 generation (Supplemental Fig. S5A-C). When *TNI*^{intron} was expressed in the lateral root initials, the number of lateral roots was reduced to ~50% in a homozygous *pPLT7::TNI*^{intron}

transgenic line (Supplemental Fig. S5B and D), a reduction that is similar to what was observed in the *tni* allele (Fig. 1L). These results suggest that fewer lateral roots in *tni* is caused by the local loss of UBP14 activity in the lateral root initials.

TNI^{intron} lacks de-ubiquitinase activity

To test whether the mutant protein retains enzymatic activity, we compared TNI with TNI^{intron} through an *in vitro* de-ubiquitination assay (Doelling et al., 2001; Rao-Naik et al., 2000). Recombinant TNI efficiently cleaved 2–7-mer Lys48-linked poly-ubiquitin substrates into mono-ubiquitin (Supplemental Fig. S6A). However, TNI^{intron} as well as the catalytically inactive UBP14^{C317S}control protein (Doelling et al., 2001) failed to cleave poly-ubiquitin substrates. TNI^{intron} and TNI^{C317S} also failed to cleave *UBQ10*-encoded α-linked hexa-ubiquitin chains in *E. coli* cells (Rao-Naik et al., 2000), whereas hexa-ubiquitin substrate was completely cleaved into di- and mono-ubiquitin forms by TNI and UBP14 from yeast, a functional homolog of TNI (Supplemental Fig. S6B) (Amerik et al., 1997). A similar *in vivo* de-ubiquitination assay in *E.coli* cells expressing α-linked, His-tagged tetra-ubiquitin (Rao-Naik et al., 2000) also showed that TNI, but not TNI^{intron}or TNI^{C317S}, cleaves the substrate into His-tagged di- and mono-ubiquitin products as detected by anti-His antibody (Supplemental Fig. S6C). Together, these results show that TNI^{intron} is catalytically inactive towards iso-linked and α-linked poly-ubiquitin substrates.

Increased accumulation of poly-ubiquitin and poly-ubiquitinated proteins in *tni*

Western blot analysis of the total protein samples from Col-0 and *tni* plants using anti-ubiquitin antibody showed reduced mono-ubiquitin and an excess accumulation of poly-ubiquitinated proteins in *tni* (Supplemental Fig. S7A and B). In line with the lack of catalytic activity in TNI^{intron}, free poly-ubiquitin chains were detected only in *tni* plants (Supplemental Fig. S7A), as was reported earlier for other *ubp14* alleles (Doelling et al., 2001; Xu et al., 2016). In Arabidopsis, the most abundant Lys48-linked poly-ubiquitin is implicated in protein turn-over through the 26S proteasome,whereas Lys63-linked poly-ubiquitin imparts non-degradative fate to the cellular proteins (Kim et al., 2013; Mevissen and Komander, 2017). Western blot analysis of the total protein extracts using linkage-specific antibodies showed a higher abundance of Lys48-linked poly-ubiquitinated proteins, and not Lys63-linked proteins, in *tni* seedlings relative to Col-0 (Fig. 6A and B), suggesting that TNI is involved in the turn-over of the cellular proteins by ubiquitin-26S proteasomaldegradation. These ubiquitin antibodies did not recognize mono-ubiquitin since it lacks such linkages.

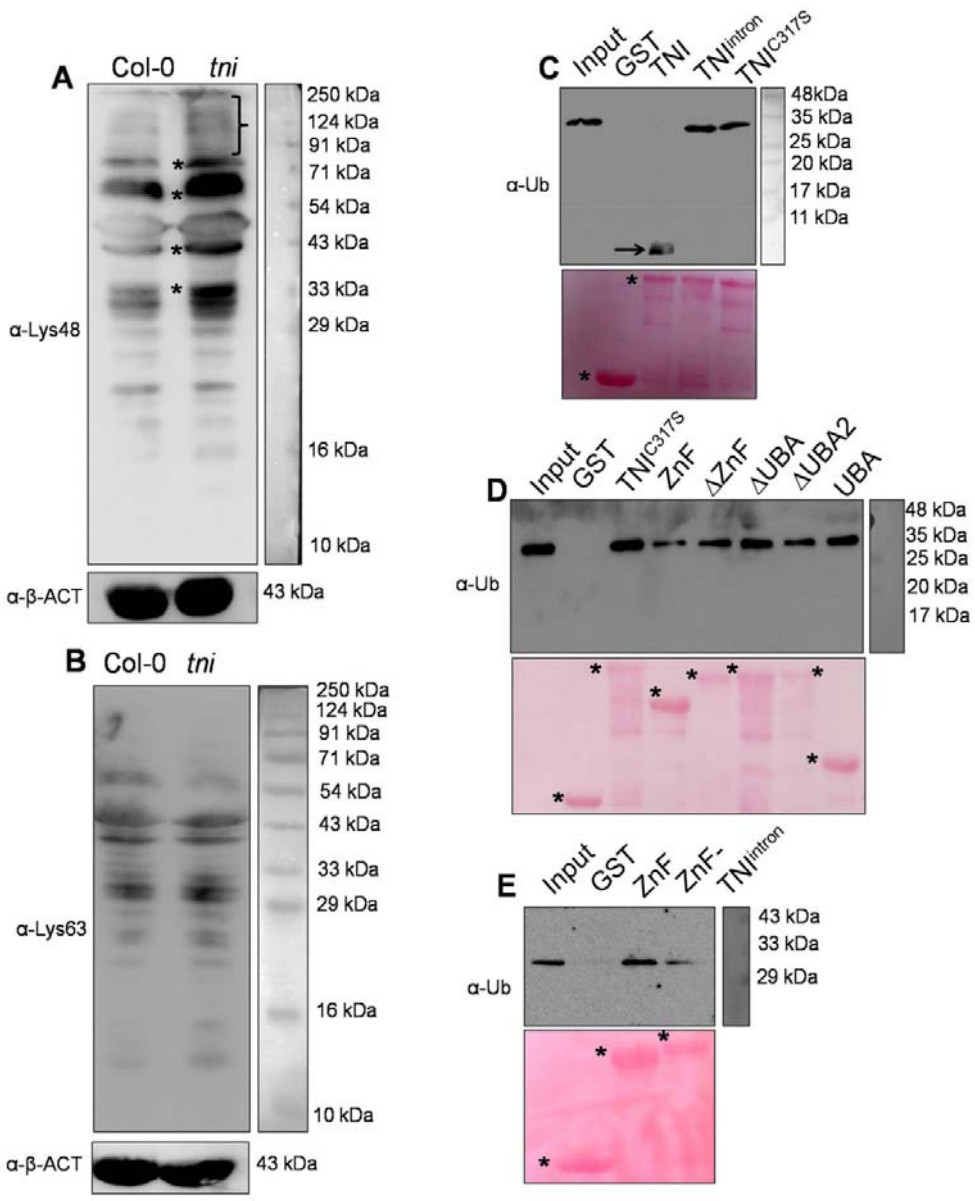

Figure 6. Linkage specificity and ubiquitin binding by TNI. (A and **B)** Western blots of total proteins extracted from 7-day-old seedlings probed with anti-ubiquitin antibody specific to Lys48 (α-Lys48) (**A**) or Lys63 (α-Lys63) (**B**) linkage. Bracket and * in (**A**) indicate smear of Lys48 linked poly-ubiquitinated proteins and α-β-ACTIN (α-β-ACT) served as loading control. **(C-E)** Anti-ubiquitin (α-Ub) Western blots of Lys48-linked tetra-ubiquitin substrate incubated with recombinant, GST-tagged full-length (TNI, TNI^{intron}, and TNI^{C317S} in **C** and **D**), and truncated (ZnF, ΔZnF, ΔUBA, ΔUBA2, UBA, and ZnF-TNI^{intron} in **D** and **E**) forms of TNI protein immobilized on glutathione beads. Lys48-linked tetra-ubiquitin substrate alone (Input) and recombinant GST protein served as positive and negative controls, respectively. Arrow in (**C**) indicates mono-ubiquitin product. Ponceau-stained membranes shown below served as loading control wherein asterisks denote the recombinant proteins used for the assays.

To determine whether proteasomal activity is altered in *tni*, we compared the sensitivity of Col-0 and *tni* seedlings to MG132, a proteasome inhibitor. Poly-ubiquitinated protein signal was more intense in *tni* than in Col-0 at 0, 0.1, and 0.2 mM MG132 (Supplemental Fig.S7C

342 and D), suggesting that the *tni* cells are hyper-sensitive to the perturbation of proteasomal
343 activity. Interestingly, MG132 treatment did not alter the steady-state level of free poly-
344 ubiquitin chains in *tni* (Supplemental Fig. S7C), suggesting that their accumulation is caused
345 by their inefficient hydrolysis by TNI^{intron}. Indeed, incubation of total protein extract from *tni*
346 seedlings with recombinant TNI, but not with TNI^{intron} or TNI^{C317S}, resulted in the
347 disappearance of the free poly-ubiquitin chains with concomitant accumulation of mono-
348 ubiquitin (Supplemental Fig. S8), resulting in a Western blot profile somewhat similar to the
349 Col-0 profile (Supplemental Fig. S7A).

350 **TNI^{intron} binds to poly-ubiquitin substrate**

351 To examine whether the 34-residue insertion in TNI^{intron} interferes with its substrate-binding
352 ability, we compared the interaction of various forms of TNI with Lys48-linked tetra-
353 ubiquitin (Fig. 6C-D). Bead-bound GST-tagged, recombinant TNI, TNI^{intron}, and TNI^{C317S}
354 were incubated with Lys48-linked tetra-ubiquitin substrate and the precipitate was analysed
355 through Western blot analysis using anti-ubiquitin antibody. Each of the three forms of the
356 protein bound to the substrate, whereas only TNI cleaved the tetra-ubiquitin into mono-
357 ubiquitin (Fig. 6C). Thus, retention of the 3^{rd}intron in TNI^{intron} does not interfere with
358 substrate binding.

359 To map the poly-ubiquitin binding domains of TNI, we generated and expressed five
360 truncated forms of TNI in *E. coli*(Supplemental Fig. S9): (i) N-terminal ZnF domain alone
361 (ZnF), (ii) TNI without ZnF (ΔZnF), (iii) TNI without UBA domains (ΔUBA), (iv) TNI
362 without UBA2 (ΔUBA2), and (v) only the two UBA domains (UBA). Since full-length TNI
363 efficiently hydrolysed poly-ubiquitin into monomer (Fig. 6C) and therefore cannot be used as
364 a positive control for the binding study, we instead used TNI^{C317S} (Fig. 6C). In Western blot
365 analysis of *in vitro* substrate-binding assay, all the truncated forms of TNI and TNI^{C317S}
366 bound to the Lys48-linked tetra-ubiquitin substrate with varying efficiency (Fig. 6D). The
367 ZnF domain of the TNI^{intron} protein in isolation (named here as ZnF-TNI^{intron}) also bound to
368 the tetra-ubiquitin substrate (Fig. 6E), albeit with reduced efficiency, suggesting that its
369 disruption does not affect its substrate-binding capability. Thus, the inability of TNI^{intron} to
370 hydrolyse poly-ubiquitin substrate is perhaps due to an overall conformational change
371 rendering the catalytic domain inactive.

372 **Increased abundance of AUX/IAA transcriptional repressors in *tni***

373 Reduced 26S-proteasome activity in *tni* may lead to an array of auxin-related growth defects
374 by stabilizing AUX/IAA repressors, similar to what is found in their gain-of-function mutants
375 (Tian and Reed, 1999; Hamann et al., 1999, Uehara et al., 2008). To test this, we compared
376 DII:VENUS signals, a readout of AUX/IAA level,of *tni* and wild-type (Fig. 7A).Weak
377 VENUS signal was detected in Col-0 primary root due to rapid turn-over of DII:VENUS,
378 which is suggestive of high auxin activity. Col-0 roots expressing a mutant, non-degradable
379 form of the protein, mDII:VENUS, showed strong and widespread VENUS signal, which is
380 consistent with previous reports (Brunoud et al, 2012). The primary roots of *DII:VENUS tni*
381 also showed VENUS signal stronger than Col-0. Western blot analysis of protein extracts
382 from 7-day-old seedlings using anti-GFP antibody further confirmed that the level of
383 DII:VENUSwas indeed more abundant in *tni* seedlings than in Col-0 (Fig. 7B).

384 The above result suggests that the DII domain, and hence some of the AUX/IAA repressors,
385 are stabilized in *tni* roots. To test this, we compared AXR3/IAA17 level in Col-0 and *tni*. The
386 heat-inducible *HS::AXR3-NT:GUS* reporter line has been extensively used to monitor IAA17
387 turn-over in various mutants in which protein degradation by 26S proteasome is affected
388 (Gray et al., 2001). We detected weak and patchy GUS signal 20 min after heat-shock
389 treatment of the *HS::AXR3-NT:GUS* seedlings, which disappeared within 80 min (Fig. 7C,
390 top panel), suggesting efficient turnover of the protein in Col-0. The non-degradable form of
391 the protein, axr3-1-NT:GUS, accumulated in the *HS::axr3-1-NT:GUS* line in large amounts
392 at 20 min and continued to accumulate, producing stronger GUS signal after 80 min (Fig. 7C,
393 middle panel). Similarly, the GUS signal in the *HS::AXR3-NT:GUS tni* cotyledons also
394 accumulated with more intensity than in Col-0, and decreased at a slower pace retaining
395 considerable signal even after 80 min of heat shock induction (Fig. 7C, bottom panel).

396 As in *tni*, reduced auxin sensitivity effects including fewer lateral roots is also seen in the
397 *iaa18-1* allele where IAA18 is stabilized (Ploense et al, 2009; Uehara et al., 2008). To
398 determine if IAA18 is stabilized in the *tni* mutant, we compared IAA18:GUS activity of *tni*
399 seedlings with Col-0. GUS signal was detected in the vasculature of cotyledons, lateral roots,
400 and primary roots in the IAA18:GUS seedlings (Fig. 7D-F). Though the pattern of the signal
401 remained more or less similar in the vasculature of the *IAA18:GUS tni* seedlings, its intensity
402 increased suggesting more IAA18 abundance in the mutant. Quantification of β-
403 glucuronidase activity also showed an increase in IAA18:GUS signal in *tni* plants (Fig. 7G).
404 Taken together, the above observations suggest that TNI is required for the turn-over of
405 certain AUX/IAA proteins.

406

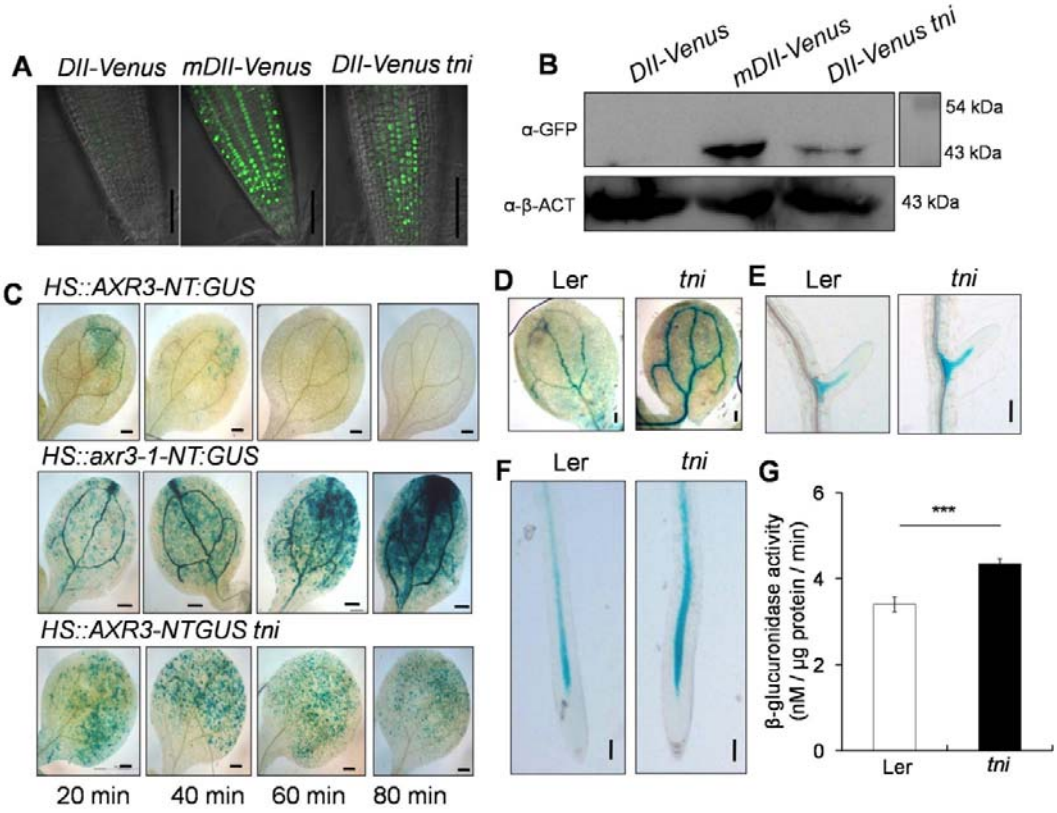

Figure 7. Stabilization of AUX/IAAs in *tni*. **(A)** DII:VENUS signal in the primary roots of 7-day-old Col-0 (*DII:VENUS* and *mDII:VENUS*) and *tni* (*DII:VENUS tni*) seedlings. Strong signal of mDII:VENUS, a non-degradable version of DII domain served as a positive control. Scale bar, 50µm. **(B)** Anti-GFP Western blot of total protein extracts from 7-day-old Col-0 (*DII:VENUS* and *mDII:VENUS*) and *tni* (*DII:VENUS tni*) seedlings. α-β-ACTIN (α-β-ACT) served as internal control. Numbers indicate molecular-weight markers. **(C)** GUS activity in the cotyledons of 7-day-old seedlings after increasing durations of heat shock. The non-degradable form *axr3-1-NT* in the middle panel served as a positive control. NT denotes N-terminal domain. Scale bar, 200µm. **(D-F)** IAA18:GUS signal in cotyledon vein (**D**), lateral root (**E**), and primary root (**F**) of *IAA18:GUS* (Ler) and *IAA18:GUS tni* seedlings. Scale bar, 200µm (**D**) and 100µm (**E-F**). **(G)** β-glucuronidase activity in *IAA18:GUS* (Ler) and *IAA18:GUS tni* (*tni*) seedlings. Averages of triplicate biological replicates are shown. Error bars represent SD. *** denotes $p<0.0001$ (unpaired Student's *t*-test).

DISCUSSION

The *tni* allele of *UBP14* is recessive and likely hypomorphic in nature as its knockout alleles show embryonic lethality. The previously reported *ttn6-4* allele, which has a deletion of 400 bp resulting in the elimination of exons 6 and 7, causes defective embryos arrested at the globular stage (Tzafrir et al., 2002). T-DNA insertions in the 7th and the 11th intron in *ubp14-1* and *ubp14-2* alleles, respectively, also yield null mutants with similar embryo phenotypes (Doelling et al., 2001). The *tni* allele also exhibited partial embryo lethality resulting in reduced seed setting (KaridasPremananda, PhD Thesis, 2014). The aborted embryos of *ubp14-1* and *ubp14-2* have higher levels of poly-ubiquitin and poly-ubiquitinated proteins (Doelling et al., 2001), implying that UBP14 is required for ubiquitin recycling, which is crucial for the progression of embryo development. Our results show that the *tni* plants also have elevated accumulation of un-anchored poly-ubiquitin chains as well as poly-ubiquitinated proteins with a concomitant reduction in mono-ubiquitin (Supplemental Fig. S7A and B). Thus, TNI/UBP14 is involved in ubiquitin recycling during post-embryonic development as well, failure of which results in multiple growth and developmental defects. The massive increase in total ubiquitin in *tni* can perhaps be explained by the reduction in the steady-state level of mono-ubiquitin, which is known to trigger increased ubiquitin biosynthesis (Park and Ryu, 2014). Indeed, poly-ubiquitin biosynthetic genes *UBQ13* and *UBQ14* are 2-fold up-regulated in *tni*, as revealed by an earlier microarray data set (Karidas et al., 2015). Detection of mono-ubiquitin in *tni* at a low abundance implies that partial de-ubiquitination activity is retained in the mutant, whereas mono-ubiquitin was not detected in the null alleles of *ubp14* (Doelling et al., 2001).

Since two transcripts corresponding to wild-type TNI and aberrant TNI^{intron} were detected in almost equal abundance in *tni* plants (Fig. 5I), it is likely that both normal and aberrant protein forms are expressed in comparable levels, assuming their translation efficiency is similar. Perhaps the lack of catalytic activity of half of the protein pool (TNI^{intron}) results in an inefficient turn-over of poly-ubiquitin into mono-ubiquitin. Recently, it was shown that the *da3-1* allele of *UBP14* has a G→T transversion at the 5′ exon-intron boundary of the last intron, generating a premature stop codon (Xu et al., 2016). The protein encoded by the *da3-1* locus is catalytically inactive since it lacks the C-terminal *His* box essential for catalysis. Our results show that UBP14 with disrupted ZnF domain (TNI^{intron}) is also catalytically inactive. However, inactive TNI^{intron} efficiently binds to the poly-ubiquitin substrates *in vitro*, suggesting that the mutant protein sequesters some of the cellular targets and acts as a

dominant negative form of wild-type TNI. Sequestration of the substrates in the *pPLT7::TNI*^{intron} transgenic line perhaps results in fewer lateral roots, an effect similar to target stabilization in the *tni* mutant due to the compromised activity of TNI.

Considering that UBPs maintain the steady-state level of mono-ubiquitin, which is an essential substrate for marking the target proteins for degradation, perturbation in their function is likely to affect multiple aspects of plant biology. Consequently, mutational analysis of 27 Arabidopsis UBPs revealed their diverse function in embryogenesis, leaf development, and organ size control (Doelling et al. 2001; Liu et al., 2008; Majumdar and Nath, 2020). Complete loss of UBP14/19results in embryo lethality, whereas disruption of the de-ubiquitination activity of UBP14 in the hypomorphic *da3-1* allele results in increased ploidy and enlarged organs (Xu et al., 2016). UBP26 de-ubiquitinates H2B in the nucleus, which is required for gene silencing, and its loss severely affects seed development (Sridhar et al., 2007; Luo et al., 2008). Mutant alleles of UBP15 produce narrow, serrated leaves (Liu et al. 2008). Apart from these few examples, single mutants of other UBPs do not show discernible phenotypic changes, suggesting functional redundancy. For example, UBP12 and UBP13 together promote root meristem development by stabilizing ROOT MERISTEM GROWTH FACTOR1 receptor (RGFR1) and RGFR2 (An et al., 2018). Besides, they remove ubiquitin marks from poly-ubiquitinated MYC2 *in vitro* and promote JA response (Jeong et al., 2017). These recent studies demonstrate the substrate specificity of UBPs and their pre-eminent role in plant development (Majumdar and Nath, 2020). Therefore, it is not surprising to see multiple phenotypic defects in the *tni/ubp14* mutant.

Most phenotypic defects in *tni* resembled those with compromised auxin response. For example, the rootless phenotype of *tni* is similar to that of *bdl/IAA12* gain-of-function and *mp/arf5* loss-of-function mutants (Hamann et al., 1999, 2002).The stabilized form of IAA12 in the *bdl* mutant blocks auxin-dependent ARF5 activation,which is required for hypophysis specification and root initiation (Schlereth et al, 2010). Similarly, venation patterning defects are also reported in *mp* and *bdl* mutants (Berleth et al., 2000). Reduced vein complexity in *tni* cotyledons could be either due to a reduced auxin transport or signaling. However, we did not see any significant difference in expression of the auxin transporter *PIN1* between Col-0 and *tni* (Supplemental Fig. S10). Another major auxin-related defect in *tni* is fewer lateral roots, a phenotype also seen in plants with stabilized AUX/IAAs such as IAA3, 14, 18, 19, and 28 (Tian and Reed, 1999; Fukaki et al., 2002; Uehara et al., 2008). Gain-of-function mutation in these repressors either produce no, or very few, lateral roots. *ARF7* and *19* act downstream to

IAA14/SLR to promote lateral root initiation (Okushima et al, 2005, 2007). Genetic interaction of *tni* with *arf7-1* showed an additive effect in lateral root emergence, which can be interpreted as both these genes working in parallel pathways. However, it should be notedthat *ARF19* compensates for the loss of *ARF7* function in *arf7-1*, which shows a much weaker phenotype compared to *arf7-1 arf19-1* double mutant. Moreover, the hypomorphic nature of *tni* allele may contribute to the additive phenotype of the *arf7-1 tni* double mutant, and perhaps in *tir1-1 tni* and *aux1-7 tni* mutants as well. Besides, *tir1-1* and *aux1-7* are also weak alleles, and combination of two weaker alleles is expected to show an additive phenotype, even if they work in the same pathway.

One possible mechanism of reduced auxin response in *tni* could be the stabilization of AUX/IAAs including IAA17 and 18 (Fig. 7). The Arabidopsis genome encodes 29 AUX/IAAs with a conserved domain II (DII), which interacts with TIR1 and undergoes poly-ubiquitination and degradation by the 26S proteasome with varying kinetics (Gray et al., 2001; Reed, 2001). Increased DII:VENUS signal in *tni* is in agreement with the stabilization of multiple AUX/IAAs. However, our study falls short of providing direct evidence that the *tni* phenotype is mediated by AUX/IAA stabilization. It also does not resolve whether AUX/IAAs in *tni* are stabilized in the free form or in the poly-ubiquitinated form. It is possible that accumulation of Lys48-linked free poly-ubiquitin chains creates a road-block for protein degradation by the 26S proteasome, as reported in yeast and human (Amerik et al., 1997; Dayal, et al., 2009), leading to an increase in poly-ubiquitinated target proteins. Direct measurement of poly-ubiquitinated AUX/IAAs in wild-type and *tni* would be required to determine whether they are part of this protein pool.

Since degradation of negative regulators by the ubiquitin-proteasome pathway is a general theme of signalingfor several plant hormones, it is likely that the response pathways of other hormones would also be affected in *tni*. For example, the DELLA proteins that suppress GA signaling are also degraded by the 26S proteasome pathway (Daviere and Archard 2013; Wang and Deng, 2011) and hence are likely to be stabilized in the *tni* mutant. Whereas this is expected to cause reduced GA response in the mutant, we had earlier noticed an elevated GA-related phenotype in *tni*, which was rescued by inhibiting GA synthesis (Karidas et al., 2015). It is possible that stabilized DELLA proteins in the mutant suppress GA signalingto an extent that triggers increased GA biosynthesis as a feedback response (Nelson and Steber, 2016). Ubiquitin-dependent degradation of hormone repressors may not be the only mechanism of action for TNI. It has been recently shown that UBP14 interacts with the ULTRAVIOLET-B

INSENSITIVE 4 protein in repressing endoreduplication and organ growth in Arabidopsis (Xu et al., 2016). Interestingly, both GA signalling and low-auxin response promotes entry into the endocycle (Gendreau et al., 1999; Ishida et al., 2010). Thus, the collective phenotypic defects in *tni* could be a cumulative effect of multiple pathways.

CONCLUSIONS

We show that *TNI* encodes the UBP14 enzyme, whose activity is partly compromised in the *tni* mutant since the mutation causes inefficient splicing of the *TNI* transcript. This results in an aberrant proteinthat lacks catalytic activity, leading to an accumulation of poly-ubiquitin chains and excess poly-ubiquitinated proteins. This is accompanied bywidespread auxin-deficient phenotypesand the stabilization of certain AUX/IAA repressors.

MATERIALS AND METHODS

Plant materials

Arabidopsis thaliana ecotypes Col-0 and L*er* were used as wild-type. The mutant/transgenic lines *DR5::GUS* (Ulmasov et al., 1997), *DR5::nYFP* (Mähönen et al., 2015), *IAA2::GUS* (Marchant, et al., 2002), *HS::AXR3-NT:GUS* (N9571), *HS:axr3-1-NT:GUS* (N9572) (Gray et al., 2001), *DII-VENUS* (N799173), *mDII-VENUS* (N799174) (Brunoud et al., 2012), *IAA18:GUS* (Ploense et al., 2009), *arf7-1* (CS24607) (Okushima et al, 2005), *aux1-7* (CS3074) (Swarup et al, 2004), *tir1-1* (CS3798) (Ruegger et al, 1998), and *ttn6-4* (CS16079) (Tzafrir et al., 2002) have been reported earlier. Most of these lines were obtained from the Nottingham Arabidopsis Stock Center (NASC, UK) or from Arabidopsis Biological Resource Center (ABRC, USA).

Plant growth conditions and treatments

Seeds were surface sterilized and stratified in darkness for 2 days at 4°C following which they were transferred to the growth chamber and maintained under long-day conditions with 16 h light (120 µmol/m^2/s) and 8 h dark, 22°C. For 1-NAA (Sigma, USA) and NPA (Calbiochem, Germany) sensitivity assays, seedlings were grown for 4 days in NAA/NPA-free ½MS medium supplemented with 1% (w/v) sucrose (Sigma, USA) and 0.8% agar (Hi Media, India), transferred to 1-NAA- or NPA-containing MS plates and placed vertically in a growth chamber for an additional 3 (for NAA) or 5 (for NPA) days. Photographs were taken at 7 or 9 days after germination and lateral roots were counted using a differential

interference contrast (DIC) microscope (Olympus, JAPAN). 7-day-old seedlings were treated with MG132 (Sigma, USA) for 16 h in liquid medium containing ½ MS salt.

Gravitropism assay

A gravitropic response assay was performed according to protocol described earlier (Hobbie et al, 2000). Briefly, ½ MS plates containing the seeds were kept vertically in a growth chamber and rotated clockwise by 90° 4 days after germination. ImageJ software (*rsbweb.nih.gov/ij/)* was used to measure the angle of curvature after 3 days of gravistimulation.

Tissue clearing

Seedlings were kept in 70% (v/v) ethanol for 24 h, incubated in lactic acid for 30 min, and then mounted in lactic acid on a transparent glass slide and observed under a DIC microscope.

Embryo dissection

Fertilized ovules were scooped out from siliques and placed on a glass slide containing Hoyer's medium (HM) and chloralhydrate:glycerol:water in a 8:1:2 ratio. Images were acquired using a Zeiss Axio Imager M1 microscope with DIC settings (Zeiss, Germany).

Map-based cloning

tni in Col-0 background was crossed to L*er* and the F_2 individuals resembling *tni* were selected. Genomic DNA was extracted from the inflorescence of these individuals using Nucleon Phytopure kit (GE HealthCare, USA). *Polymorph* (www.polymorph.weigelworld.org) and *dCAPSFinder (http://helix.wustl.edu/dcaps/dcaps.html)* software were used to design CAPS and dCAPS markers (Supplemental Table S1). The *tni* locus was mapped to a 65-kb genomic region with the help of these markers and 509 *tni* mapping individuals. Among 21 genes in this interval, the candidate genes were amplified and cloned into the *pGEM-T-Easy* vector (Promega, USA), followed by Sanger DNA sequencing.

Generation of constructs and transgenic lines

TNI coding sequence was amplified by PCR from cDNA using primers P1888 and P1889 (Supplemental Table S2). To generate the *TNI* over-expression construct *35S::TNI*, the

coding sequence was cloned downstream of the *35S CaMV* promoter in *pCAMBIA1302*. *TNI*^{intron} of amplicon size 800 bp was amplified from *tni* cDNA with primers P1888 and P1774 harboring BglII and BsmI restriction sites and cloned into *pGEM-T-Easy-TNI* to make *pGEM-T-Easy-TNI*^{intron}. With BglII and BsmI restriction enzymes, the first 414 bp of *TNI* in *35S::TNI* (*pCAMBIA1302*) was replaced with *TNI*^{intron} from *pGEM-T-Easy-TNI*^{intron} to generate *35S::TNI*^{intron} (*pCAMBIA1302*). The 35S promoter in*35S::TNI*^{intron} was replaced with *RPS5a* promoter, which was amplified with primers P2230 and P2231 harboring BamHI and BglII sites to obtain*RPS5a::TNI*^{intron}.

Artificial microRNA against *TNI* was designed as per the protocol described earlier (*http://wmd3.weigelworld.org/cgi-bin/webapp.cgi*). Briefly, primers P1918, P1919, P1920, and P1921 were used to clone the amiR fragment and subsequently cloned into *pGEM-T-Easy* vector. Primers P2887 and P2888 were used to amplify *amiR-TNI* and cloned into pCAMBIA1302. The *35S CaMV* promoter of *pCAMBIA1302* was replaced with RPS5a promoter to generate *RPS5a*::*amiR-TNI* (*amiR-TNI*). The *RPS5a* promoter sequence was amplified with P2231 and P2238. For *pPLT7::TNI*^{intron}, the *35SCaMV* promoter was replaced with 1.5-kb *pPLT7* in pCAMBIA1302 and pCAMBIA1390 using the primers P2801 and P2802. The CDS of *TNI*^{intron} was cloned downstream to the *pPLT7* in *pCAMBIA1302* to make the construct *pPLT7::TNI*^{intron}. The *PLT7::amiR-TNI* construct was generated similarly. To make the transcriptional fusion of *TNI*, 1.9-kb upstream region of *TNI* locus was amplified using primers P2759 and P2760 and cloned into pDONR221. The promoter sequence was cloned into pMDC162 destination vector to make the *pTNI::GUS* construct.

Agrobacterium GV3101 was transformed with these constructs by electroporation. Flowering Arabidopsis plants were transformed with *Agrobacterium* harboring individual constructs through the floral dip method (Clough and Bent, 1998).

TNI CDS was cloned in *pGEX-4T-1* using primers P1912 and P1913 with engineered BamH1 and SalI restriction sites respectively to create the *pGEX4-T-1-TNI* construct. *pGEX4T-1-TNI*was replaced with *TNI*^{intron} using SacI and HindIII restriction enzymes to make the *pGEX4T-1-TNI*^{intron} construct. *TNI*^{C317S} mutant was generated using Q5 site-directed mutagenesis kit (NEB, USA). *pGEM-T-Easy-TNI* served as a template for making the site-directed mutant using primers P2346 and P2347. *TNI* fragment in *pGEM-T-Easy-TNI* was replaced with *TNI*^{C317S} using BglII and SpeI to create *pGEM-T-Easy-TNI*^{C317S}. From this vector, the *TNI*^{C317S} coding sequence was moved to *pGEX4-T-1* using BamH1 and SalI

restriction enzymes for protein expression. The *pGEX-4T-1-TNI* was used as the template to generate truncated proteins ZnF, ΔZnF, ΔUBA, ΔUBA2, and UBA domains using primer pairs P1912, P2405; P2403, P1913; P1912, P2549; P1912, P2806; and P2827, P2808 respectively with engineered BamH1 and Sal1 restriction sites. All these deletion constructs were subsequently cloned into *pGEX-4T-1*.

Purification of GST-tagged recombinant proteins from *E.coli*

Recombinant protein expression and purification was done according to the protocol previously described (Harper and Speicher, 2011)with some modifications. Briefly, transformed *E.coli*(BL21)cells were induced with 0.5 mM IPTG (Sigma, USA) at mid-log phase, incubated at 16°C for 12 h, harvested by centrifugation at 4000g for 5 min at 4°C, and suspended in lysis buffer (50 mM Tris-HCl pH 7.4, 150 mM KCl, 0.5 mM EDTA, 10% (v/v) glycerol, 0.5% (v/v) NP-40, 1 mM PMSF and protease inhibitor cocktail) followed by sonication until it turned clear. Clear supernatant was collected after centrifugation at 12,000g for 20 min at 4°C and incubated with glutathione beads (Novagen, USA) for 2 h at 4°C with constant shaking. Beads were washed five times with ice-cold cell suspension buffer, and bound protein eluted with 2 mM glutathione. SDS-PAGE was used to analyse the proteins.

***In vitro* and *in vivo* de-ubiquitination assay**

De-ubiquitination assays were performed as described earlier (Rao-Naik et al., 2000). Briefly, a 50-µl assay reaction comprising purified protein, 50 mM Tris-HCL pH 8, 150 mM NaCl, 10 mM β-mercaptoethanol, 0.5 mg/ml BSA, and 2µg 2–7-mer of poly-ubiquitin (Boston Biochemical, USA) was incubated at 37°C for 3 h. Laemlli buffer (200mMTris-HCl pH-6.8, 10% (w/v) SDS, 30% (v/v)glycerol 0.05% (v/v) bromophenol blue, and β-mercaptoethanol) was added to stop the reaction. Assay mixture was fractionated by SDS-PAGE and immunoblot analysis was performed using anti-ubiquitin antibody (Novus Biologicals, USA). For *in vivo* assays, *E.coli* was co-transformed with constructs along with the p8190-UBQ10 and pACYC184-Ub_4 constructs (Rao-Naik et al., 2000), induced with 0.5 mM IPTG, and incubated for 3 h at 37°C. Equal cell aliquots were pelleted down, suspended into lysis buffer, and sonicated until clear. Supernatant was boiled inLaemlli buffer and analysed by SDS-PAGE. Immunoblotting was done using anti-ubiquitin and anti-His antibodies (Sigma, USA).

***In vitro* substrate binding assay**

GST-tagged recombinant proteins were purified using glutathione sepharose beads as mentioned in the previous section. 5–50 µl bead-bound protein was incubated with 1µg Lys48-linked tetra-ubiquitin (Boston Biochemicals, USA) in sodium phosphate, pH 7.4 in the presence of a protease inhibitor cocktail (Roche, Germany). The reaction mixture was incubated at 4°C for 2 h with shaking, then stopped by the addition of Laemlli buffer and boiling the sample for 10 min. The reaction mixture was fractionated by SDS-PAGE and immunoblotting was performed using anti-ubiquitin antibody.

GUS staining and MUG assay

GUS staining was performed as described earlier (Karidas et al., 2015). Seedlings were harvested in ice-cold 90% (v/v) acetone, incubated on ice for 20 min, and then in staining buffer (0.5 M sodium phosphate buffer pH 7.2, 10% (v/v) Triton-X, 100 mM potassium ferrocyanide, and 100 mM potassium ferricyanide) for 20 min at 25C. 2 mM X-Gluc (Thermo Scientific, USA) was added to the fresh staining buffer containing seedlings and incubated at 37°C for up to 12 h, followed by washing with 70% (v/v) ethanol for 30–60 min at 25°C until chlorophyll was removed, mounting on a glass slide in lactic acid, and observations under DIC microscopy.

MUG assayswere performed according to the previously described protocol (Weigel and Glazebrook, 2002). Briefly, protein was extracted from seedlings using extraction buffer (50 mM sodium phosphate pH 7.0, 10 mM EDTA, 0.1% (w/v) SDS, 0.1% (v/v) TritonX-100, 1 mM PMSF, and protease inhibitor cocktail), centrifuged at 12,000g at 4°C for 15 minafter which clear supernatant was collected and equal concentration of proteins was taken for the MUG assay. The MUG assay buffer composition is that of the extraction buffer supplemented with 1 mM MUG (Sigma, USA). Reactionswere incubated at 37°C for 20 min and stopped using 0.2 M sodium carbonate. A TECAN fluorimeter was used to measure the fluorescence at 365nm excitation and 455nm emission wavelengths.

Antibody generation

Anti-TNI polyclonal antibody was raised against a synthetic peptide (USV Ltd, India) corresponding to residues 156–174 of TNI/UBP14, which was identified as a potent immunogen using the software available at http://tools.iedb.org/main/bcell/. 5 mg synthetic peptide with>85% purity was conjugated to Keyhole limpet haemocyanin carrier. Rabbits

were immunized with 1mg conjugated peptide, followed by 3 booster immunizationseach with500 µg conjugated peptide. Post immunization anti-serum was collected from the rabbits.

Immunoblot analysis

Proteins were isolated from 7–8-day-old seedlings using protein extraction buffer (50 mM Tris-HCl pH 7.4, 300 mM KCl, 0.5 mM EDTA, 10% (v/v) glycerol, 0.5% (v/v) NP-40) along with 1 mM PMSF, 50µM MG132, and complete protease inhibitor cocktail (Roche, Germany). Extract was cleared by centrifugation at 12,000gfor 15 min at 4°C. Equal concentrations of protein were analysed in 15% or 10% (v/v) SDS-PAGE, transferred to PVDF membranes (Millipore, USA), and immunoblotted using anti-GFP (Roche, Germany), anti-ubiquitin, anti-Lys48 ubiquitin (CST, USA), and anti-Lys63 (Enzo Life sciences, USA) antibodies. ECl (Millipore, USA) was used to develop the blots.

Confocal microscopy

Roots were stained with 10µg/mL propidium iodide (Sigma, USA) for 5 min, mounted on a glass slide, and observed under a laser confocal microscope (Zeiss LSM 710, Germany).

RNA isolation and cDNA synthesis

Total RNA was extracted from 7-day-old seedlings using Trizol (Sigma, USA), treated with DNase (Fermentus, USA) for 2 h at 37°C, and precipitated by sodium acetate. 2µg RNA was used as template for cDNA preparation using Revert Aid M-MuLV reverse transcriptase (Fermentus, USA). 20-µl reverse transcription reactions were set up and the amplified products were visualized using ethidium bromide staining of 1% (w/v) agarosegels.

ACCESSION NUMBERS

The accession numbers of the genes mentioned in this article are given below and their sequence data can be found in Arabidopsis genome initiative (www.arabidopsis.org): *IAA2* (*At3G23030*), *AXR3*(*At1G04250*), *IAA18* (*At1G51950*), *ARF7* (*At5G20730*), *AUX1* (*At2G38120*), *TIR1* (*At3G62980*), *PIN1 (At1G73590*), and *TTN6* (*At3G20630*).

SUPPLEMENTAL DATA

Supplemental Figure S1. Pro-embryo and cotyledon phenotype in *tni*.

687 **Supplemental Figure S2. Differentially expressed auxin-related genes in *tni*.**

688 **Supplemental Figure S3. Cloning of the *tni* locus.**

689 **Supplemental Figure S4. Tissue specific expression of *TNI* promoter.**

690 **Supplemental Figure S5. Effects of *TNI* mis-expression on lateral roots.**

691 **Supplemental Figure S6. TNI^{intron} is catalytically inactive**.

692 **Supplemental Figure S7**. **Accumulation of poly-ubiquitinated proteins in *tni* mutant**.

693 **Supplemental Figure S8. *In vitro* disassembly of ubiquitin conjugates from *tni* plant**
694 **extract.**

695 **Supplemental Figure S9. Expression of recombinant TNI protein in *E. coli*.**

696 **Supplemental Figure S10. *PIN1::GUS* reporter assay in *tni*.**

697

698 **Supplemental Table S1.** List of markers used for fine mapping of *TNI* locus along with their
699 nature and positions in the genome.

700 **Supplemental Table S2.** List of primers used for generating constructs.

701

702

703 **ACKNOWLEDGEMENTS**

704 We acknowledge B. Vijaya Lakshmi Vadde (Indian Institute of Science, India) for anti-TNI
705 antibody, M. Sowmya Spandana (Indian Institute of Science, India) for help in making
706 clones, Jason Reed (University of North Carolina, US) for *IAA18:GUS*, Judy Callis
707 (University of California, US) for *ScUBP14*, Ub_6 and *His-*Ub_4 constructs, Ben Scheres
708 (Wageningen University, Netherlands) for *DR5::GUS* and *DR5::nYFP* lines, Kalika Prasad
709 (IISER Thiruvananthapuram, India) for *pPLT7* construct and P. Ajit Kumar (Indian Institute
710 of Science, India) for access to Zeiss microscope.

711 **Figure 1. Auxin-related phenotypes in *tni*. (A)** 2-cell pro-embryo. Arrows highlight vertical
712 (Col-0) or horizontal (*tni*) cell division. **(B)** 1-cell pro-embryo. Arrow indicates periclinal cell
713 division defect in the *tni* basal cell. **(C)** Globular stage embryo. Normal (Col-0) and aberrant
714 (*tni*) lens-shaped cells are magnified in the insets. Scale bar (in **A**-**C**), 10μm. **(D)** Normal
715 (Col-0) and rootless (*tni*) seedlings. Scale bar, 1mm.The image was digitally extracted to

716 remove the background. **(E)** 7-day-old seedlings with two (Col-0) or three (*tni*) cotyledons.
717 Scale bar, 1mm. The photograph is taken in a black background. **(F)** Heart stage embryo with
718 two (Col-0) or three (*tni*) cotyledon primordial (marked by dotted line). Col-0 meristem is
719 falselycolored in yellow. Scale bar, 10μm. **(G)** Cotyledons from 7-day-old seedlings are
720 cleared to highlight veins. Open venation in *tni* is marked by arrows. Scale bar, 1 mm. **(H)**
721 Percentage of cotyledons (n= 103 in Col-0 and 90 in *tni*) showing closed or open veins. **(I)**
722 Effect of gravistimulation on primary roots of 7-day-old seedlings. Angles of root bending
723 are indicated by red lines. Scale bar, 5 mm. **(J)** Average angle of curvature (n= 52 for Col-0
724 and 43 for *tni*) of primary roots following gravistimulation shown in (**I**). Error bars represent
725 SD. *** denotes p<0.0001 (unpaired Student's *t*-test was used). (**K**) 11-day-old seedlings.
726 Scale bar, 5 mm. **(L)** Average number of lateral roots (n= 10–13) in seedlings at indicated
727 days after germination (DAG). Error bars represent SD. *** denotes p<0.0001 (unpaired
728 Student's *t*-test). **(M)** Open flowers showing variation in petal number in *tni* mutant. The
729 image was digitally extracted to remove the background. (**N)** Matured seeds. Scale bar, 1
730 mm. (O) Average seed area (n= 15). Error bars represent SD. *** denotes p<0.0001
731 (unpaired Student's *t*-test).

732 **Figure 2. Auxin response in *tni*. (A-D)** DR5::GUS activity in the cotyledons (**A**), first leaf
733 pair **(B)**, primary root tips **(C),** and lateral root tips **(D)** of 3-**(A)** and 7-day-old (**B**-**D**)
734 *DR5::GUS* (Col-0) and *DR5::GUS tni* (*tni*) seedlings. Scale bar, 200μm (**A**, **B**) and 100μm
735 (**C**, **D)**. **(E** and **F)** DR5::nYFP signal at the tips of cotyledons of 5-day-old seedlings (**E**) and
736 primary roots (**F**) of 7–8-day-old *DR5::nYFP* (Col-0) and *DR5::nYFP tni* (*tni*) seedlings.
737 Scale bar, 50μm (**E**, **F**). Root samples were stained with propidium iodide in (**F**). **(G)**
738 Western blots of the total proteins from 7-day-old *DR5::nYFP* (Col-0) and *DR5::nYFP tni*
739 (*tni*) seedlings. α-β-ACTIN (α-β-ACT) was used as a control. **(H)** β-glucuronidase activity
740 estimated in total extracts of *DR5::GUS* (Col-0) and *DR5::nYFP tni* (*tni*) seedlings. Averages
741 of three biological replicates are shown. Error bars represent SD. * indicates p=0.0406
742 (unpaired Student's *t*-test). **(I-K)** IAA2::GUS activity in the cotyledons (**I**), first leaf pairs **(J)**
743 and primary roots **(K)** of 7-day-old *IAA2::GUS* (Col-0) and *IAA2::GUS tni* (*tni*) seedlings.
744 Arrows in (**I**) indicate IAA2::GUS activity at cotyledon tips. Scale bar, 200μm (**I**, **J**) and
745 100μm **(K)**.

746 **Figure 3. Auxin sensitivity of *tni* mutant.** (**A and B**) Average number of lateral roots of 7-
747 day-old seedlings grown in the presence of 1-naphthaleneacetic acid (NAA) (**A**) and their
748 relative increases (**B**). Error bars represent SD. Statistical analysis was done using unpaired

Student's *t*-test. *** denotes p≤0.0001. ns, not significant. **(C and D)** Average number of lateral roots in 9-day-old seedlings treated with N-1-naphthylphthalamic acid (NPA) and their relative decreases (**D**). For (**A** and **C**), n= 12–15; error bars represent SD; *** and * denote p≤0.0001 and <0.006, respectively (unpaired Student's *t*-test); ns, not significant.

Figure 4. Genetic interaction between *tni*and mutants with auxin-related defects. (A-C) Average number of lateral roots (n= 10–15) of 9-day-old seedlings. Error bars represent SD. *** denotes p<0.0001, ** denotes p= 0.0084 (unpaired Student's *t*-test), ns, not significant.

Figure 5. Cloning of *TNI*. (A) A schematic representation of *TNI*/*UBP14* locus showing 5′ UTR (black box), exons (grey box), introns (black line), and 3′ UTR (white box). Positions of T-DNA insertion in various mutant alleles are shown by inverted triangles. The *G→A* transition at the third intron-exon junction in *tni* allele and *G→T* substitution at the nineteenth exon-intron junction in the *da3-1* allele are indicated. **(B-F)** 30-day-old rosettes of wild-type (**B**)**,** *tni* (**C**), *tni* x *ttn6-4* (+/-) F_1 plants (**D**), *tni* plants over-expressing *TNI* transcript (**E**), and Col-0 plant expressing artificial microRNA (amiR) against *TNI* transcript (**F**). Red arrows indicate leaf curvature. Scale bar, 0.5 cm.The rosette images in **(B-F)** were digitally extracted to remove the background.**(G)** Schematic representations of the predicted wild-type *TNI* and the mutant TNI^{intron} transcripts. Note the retention of the 3rd intron (solid line) in TNI^{intron}. Arrows indicate the position of the primers used for RT-PCR analysis. Dotted lines indicate continuity of exons. **(H)** Domain architecture of TNI and TNI^{intron} proteins. Orange box indicates a 34amino acid-residue insertion encoded by the 3rd intron. **(I)** Ethidium bromide-stained agarose gel showing the products of RT-PCR on total RNA from Col-0 (WT), mature *tni* leaves (*tni* L) and *tni* inflorescence (*tni* I). + and - indicate cDNA and RNA as PCR templates. M, DNA marker. **(J)** Western blot of total protein extracted from 7-day-old seedlings using antibody raised against a peptide corresponding to residues 156–174 of TNI. α-β-ACTIN (α-β-ACT) was used as loading control.

Figure 6. Linkage specificity and ubiquitin binding by TNI. (A and **B)** Western blots of total proteins extracted from 7-day-old seedlings probed with anti-ubiquitin antibody specific to Lys48 (α-Lys48) (**A**) or Lys63 (α-Lys63) (**B**) linkage. Bracket and * in (**A**) indicate smear of Lys48 linked poly-ubiquitinated proteins and α-β-ACTIN (α-β-ACT) served as loading control. **(C-E)** Anti-ubiquitin (α-Ub) Western blots of Lys48-linked tetra-ubiquitin substrate incubated with recombinant, GST-tagged full-length (TNI, TNI^{intron}, and TNI^{C317S} in **C** and **D**), and truncated (ZnF, ΔZnF, ΔUBA, ΔUBA2, UBA, and ZnF-TNI^{intron} in **D** and **E**) forms

781 of TNI protein immobilized on glutathione beads. Lys48-linked tetra-ubiquitin substrate
782 alone (Input) and recombinant GST protein served as positive and negative controls,
783 respectively. Arrow in (**C**) indicates mono-ubiquitin product. Ponceau-stained membranes
784 shown below served as loading control wherein asterisks denote the recombinant proteins
785 used for the assays.

786 **Figure 7. Stabilization of AUX/IAAs in *tni*. (A)** DII:VENUS signal in the primary roots of
787 7-day-old Col-0 (*DII:VENUS* and *mDII:VENUS*) and *tni* (*DII:VENUS tni*) seedlings. Strong
788 signal of mDII:VENUS, a non-degradable version of DII domain served as a positive control.
789 Scale bar, 50µm. **(B)** Anti-GFP Western blot of total protein extracts from 7-day-old Col-0
790 (*DII:VENUS* and *mDII:VENUS*) and *tni* (*DII:VENUS tni*) seedlings. α-β-ACTIN (α-β-ACT)
791 served as internal control. Numbers indicate molecular-weight markers. **(C)** GUS activity in
792 the cotyledons of 7-day-old seedlings after increasing durations of heat shock. The non-
793 degradable form *axr3-1-NT* in the middle panel served as a positive control. NT denotes N-
794 terminal domain. Scale bar, 200µm. **(D-F)** IAA18:GUS signal in cotyledon vein (**D**), lateral
795 root (**E**), and primary root (**F**) of *IAA18:GUS* (Ler)and *IAA18:GUS tni* seedlings. Scale bar,
796 200µm (**D**) and 100µm (**E-F**). **(G)** β-glucuronidase activity in *IAA18:GUS* (Ler) and
797 *IAA18:GUS tni* (*tni*) seedlings. Averages of triplicate biological replicates are shown. Error
798 bars represent SD. *** denotes $p<0.0001$ (unpaired Student's *t*-test).

799

800

801

Parsed Citations

Amerik AY, Swaminathan S, Krantz BA, Wilkinson KD, Hochstrasser M (1997) In vivo disassembly of free polyubiquitin chains by yeast Ubp14 modulates rates of protein degradation by the proteasome. EMBO J 16: 4826–4838
Pubmed: Author and Title
Google Scholar: Author Only Title Only Author and Title

An Z, Liu Y, Ou Y, Li J, Zhang B, Sun D, Sun Y, Tang W (2018) Regulation of the stability of RGF1 receptor by the ubiquitin-specific proteases UBP12/UBP13 is critical for root meristem maintenance. Proc Natl Acad Sci 115: 1123-1128
Pubmed: Author and Title
Google Scholar: Author Only Title Only Author and Title

Bennett SRM, Alvarez J, Bossinger G, Smyth DR (1995) Morphogenesis in pinoid mutants of Arabidopsis thaliana. Plant J 8: 505–520
Pubmed: Author and Title
Google Scholar: Author Only Title Only Author and Title

Berleth T, Mattsson J, Hardtke CS (2000) Vascular continuity and auxin signaling. Trends Plant Sci 32: 173–185
Pubmed: Author and Title
Google Scholar: Author Only Title Only Author and Title

Blilou I, Xu J, Wildwater M, Willemsen V, Paponov I, Friml J, Heidstra R, Aida M, Palme K, Scheres B (2005) The PIN auxin efflux facilitator network controls growth and patterning in Arabidopsis roots. Nature 433: 39-44
Pubmed: Author and Title
Google Scholar: Author Only Title Only Author and Title

Boscá S, Knauer S, Laux T (2011) Embryonic development in Arabidopsis thaliana:from the zygote division to the shoot meristem. Front Plant Sci 2: 1-6
Pubmed: Author and Title
Google Scholar: Author Only Title Only Author and Title

Brunoud G, Wells DM, Oliva M, Larrieu A, Mirabet V, Burrow AH, Beeckman T, Kepinski S, Traas J, Bennett MJ, Vernoux T (2012) A novel sensor to map auxin response and distribution at high spatio-temporal resolution. Nature 482: 103–106
Pubmed: Author and Title
Google Scholar: Author Only Title Only Author and Title

Callis J (2014) The ubiquitination machinery of the ubiquitin system. Arab B 12: e0174
Pubmed: Author and Title
Google Scholar: Author Only Title Only Author and Title

Casimiro I, Marchant A, Bhalerao RP, Beeckman T, Dhooge S, Swarup R, Graham N, Inze D, Sandberg G, Casero PJ, Bennett M (2001) Auxin transport promotes Arabidopsis lateral root initiation. Plant cell13: 843-852
Pubmed: Author and Title
Google Scholar: Author Only Title Only Author and Title

CClough SJ, Bent AF (1998) Floral dip:a simplified method for Agrobacterium-mediated transformation of Arabidopsis thaliana. Plant J 16: 735–743
Pubmed: Author and Title
Google Scholar: Author Only Title Only Author and Title

Daviere JM, Achard P (2013) Gibberellin signaling in plants. Development 140: 1147–1151
Pubmed: Author and Title
Google Scholar: Author Only Title Only Author and Title

Dayal S, Sparks A, Jacob J, Allende-Vega N, Lane DP, Saville MK (2009) Suppression of the deubiquitinating enzyme USP5 causes the accumulation of unanchored polyubiquitin and the activation of p53. J Biol Chem 284: 5030–5041
Pubmed: Author and Title
Google Scholar: Author Only Title Only Author and Title

Delarue M, Prinsen E, Onckelen HV, Caboche M, Bellini C (1998). Sur2 mutations of Arabidopsis thaliana define a new locus involved in the control of auxin homeostasis. Plant J 14: 603–611
Pubmed: Author and Title
Google Scholar: Author Only Title Only Author and Title

De Smet I (2012) Lateral root initiation:one step at a time. New phytol193: 867-873
Pubmed: Author and Title
Google Scholar: Author Only Title Only Author and Title

Doelling JH, Yan N, Kurepa J, Walker J, Vierstra RD (2001) The ubiquitin-specific protease UBP14 is essential for early embryo development in Arabidopsis thaliana. Plant J 27: 393–405
Pubmed: Author and Title
Google Scholar: Author Only Title Only Author and Title

Fukaki H, Tameda S, Masuda H, Tasaka M (2002) Lateral root formation is blocked by a gain-of-function mutation in the SOLITARY-ROOT/IAA14 gene of Arabidopsis. Plant J 29: 153–168

Pubmed: Author and Title
Google Scholar: Author Only Title Only Author and Title

Gendreau E, Orbovic V, Höfte H, Traas J (1999) Gibberellin and ethylene control endoreduplication levels in the Arabidopsis thaliana hypocotyl. Planta 209: 513-516
Pubmed: Author and Title
Google Scholar: Author Only Title Only Author and Title

Gray WM, Kepinski S, Rouse D, Leyser O, Estelle M (2001) Auxin regulates SCFTIR1-dependent degradation of AUX/IAA proteins. Nature 414: 271–276
Pubmed: Author and Title
Google Scholar: Author Only Title Only Author and Title

Hamann T, Benkova E, Bäurle I, Kientz M, Jürgens G (2002) The Arabidopsis Bodenlos gene encodes an auxin response protein inhibiting embryo patterning. Genes Dev 16: 1610–1615
Pubmed: Author and Title
Google Scholar: Author Only Title Only Author and Title

Hamann T, Mayer U, Jurgens G (1999) The auxin-insensitive bodenlos mutation affects primary root formation and apical-basal patterning in the Arabidopsis embryo. Development126: 1387-1395
Pubmed: Author and Title
Google Scholar: Author Only Title Only Author and Title

Harper S, Speicher D W (2011) Purification of proteins fused to glutathione S-tranferase. Methods
Pubmed: Author and Title
Google Scholar: Author Only Title Only Author and Title

Mol Biol 681: 259–280

Hobbie L, McGovern M, Hurwitz LR, Pierro A, Liu NY, Bandyopadhyay A, Estelle M (2000) The axr6 mutants of Arabidopsis thaliana define a gene involved in auxin response and early development. Development 127: 23–32
Pubmed: Author and Title
Google Scholar: Author Only Title Only Author and Title

Ishida T, Adachi S, Yoshimura M, Shimizu K, Umeda M and Sugimoto K (2010) Auxin modulates the transition from the mitotic cycle to the endocycle in Arabidopsis Development 137: 63-71
Pubmed: Author and Title
Google Scholar: Author Only Title Only Author and Title

Isono E, Nagel MK (2014) Deubiquitylating enzymes and their emerging role in plant biology. Front Plant Sci 5: 1–6
Pubmed: Author and Title
Google Scholar: Author Only Title Only Author and Title

Ivanchenko MG, Napsucialy-Mendivil S, Dubrovsky JG (2010) Auxin-induced inhibition of lateral root initiation contributes to root system shaping in Arabidopsis thaliana. Plant J 64: 740-752
Pubmed: Author and Title
Google Scholar: Author Only Title Only Author and Title

Jeong JS, Jung C, Seo JS, Kim JK, Chua NH (2017) The Deubiquitinating Enzymes UBP12 and UBP13 Positively Regulate MYC2 Levels in Jasmonate Responses. Plant Cell 29: 1406-1424
Pubmed: Author and Title
Google Scholar: Author Only Title Only Author and Title

Karidas, Premananda (2014) Map-based cloning and characterization of TARANI, a global regulator of Arabidopsis development. PhD thesis
Pubmed: Author and Title
Google Scholar: Author Only Title Only Author and Title

Karidas P, Challa KR, Nath U (2015) The tarani mutation alters surface curvature in Arabidopsis leaves by perturbing the patterns of surface expansion and cell division. J Exp Bot 66: 2107–2122
Pubmed: Author and Title
Google Scholar: Author Only Title Only Author and Title

Kim DY, Scalf M, Smith LM, Vierstra RD (2013) Advanced proteomic analyses yield a deep catalog of

ubiquitylation targets in Arabidopsis. Plant Cell 25: 1523–1540

Krecek P, Skupa P, Libus J, Naramoto S, Tejos R, Friml J, Zazimalova E (2009) The PIN-FORMED (PIN) protein family of auxin transporters. Genome biol10: 249.1-249.11
Pubmed: Author and Title
Google Scholar: Author Only Title Only Author and Title

Leyser HMO, Pickett FB, Dharmasiri S, Estelle M (1996) Mutations in the AXR3 gene of Arabidopsis result in altered auxin response including ectopic expression from the SAUR-AC1 promoter. Plant J 10: 403–413
Pubmed: Author and Title

Google Scholar: Author Only Title Only Author and Title

Leyser O (2018) Auxin Signaling. Plant Physiol 176: 465-479
Pubmed: Author and Title
Google Scholar: Author Only Title Only Author and Title

Liu Y, Wang F, Zhang H, He H, Ma L, Deng XW (2008) Functional characterization of the Arabidopsis ubiquitin-specific protease gene family reveals specific role and redundancy of individual members in development. Plant J 55: 844–856
Pubmed: Author and Title
Google Scholar: Author Only Title Only Author and Title

Luo M, Luo MZ, Buzas D, Finnegan J, Helliwell C, Dennis ES, Peacock WJ, Chaudhury A (2008) UBIQUITIN-SPECIFIC PROTEASE 26 is required for seed development and the repression of PHERES1 in Arabidopsis. Genetics 180: 229–236
Pubmed: Author and Title
Google Scholar: Author Only Title Only Author and Title

Mähönen AP, ten Tusscher K, Siligato R, Smetana O, Salojärvi SDTJ, Wachsman G, Prasad K,

Heidstra R, Scheres B (2015) PLETHORA gradient formation mechanism separates auxin

MajumdarP, Nath U (2020) De-ubiquitinases on the move: an emerging field in plant biology. Plant Biology 22: 563-572
Pubmed: Author and Title
Google Scholar: Author Only Title Only Author and Title

Marchant A, Bhalerao R, Casimiro I, Eklöf J, Casero PJ, Bennett M, Sandberg G (2002) AUX1 promotes lateral root formation by facilitating indole-3-acetic acid distribution between sink and source tissues in the Arabidopsis seedling. Plant Cell 14: 589–97
Pubmed: Author and Title
Google Scholar: Author Only Title Only Author and Title

Mattsson J, Ckurshumova W, Berleth T (2003) Auxin signaling in Arabidopsis leaf vascular development. Plant Physiol 131: 1327-1339
Pubmed: Author and Title
Google Scholar: Author Only Title Only Author and Title

Mevissen TET, Komander D (2017) Mechanisms of deubiquitinase specificity and regulation. Annu Rev Biochem 86: 159–192
Pubmed: Author and Title
Google Scholar: Author Only Title Only Author and Title

Nagpal P, Walker LM, Young JC, Sonawala A, Timpte C, Estelle M, Reed JW (2000) AXR2 Encodes a Member of the Aux/IAA Protein Family. Plant Physiol 123: 563–574
Pubmed: Author and Title
Google Scholar: Author Only Title Only Author and Title

Nelson SK, Steber CM (2016) Gibberellin hormone signal perception: Down-regulating DELLA repressors of plant growth and development. Annual Plant Reviews 49: 153-188
Pubmed: Author and Title
Google Scholar: Author Only Title Only Author and Title

Okushima Y, Overvoorde PJ, Arima K, Alonso JM, Chan A, Chang C, Ecker JR, Hughes B, Lui A,

Nguyen D, Onodera C, Quach H, Smith A, Yu G, Theologis A (2005) Functional genomic

analysis of the AUXIN RESPONSE FACTOR gene family Members in Arabidopsis thaliana. Plant

Cell 17: 444–463

Okushima Y, Fukaki H, Onoda M, Theologis A, Tasaka M (2007) ARF7 and ARF19 regulate lateral root formation via direct activation of LBD/ASL genes in Arabidopsis. Plant Cell 19: 118–130
Pubmed: Author and Title
Google Scholar: Author Only Title Only Author and Title

Park CW, Ryu KY (2014) Cellular ubiquitin pool dynamics and homeostasis. BMB Rep 47: 475–482
Pubmed: Author and Title
Google Scholar: Author Only Title Only Author and Title

Ploense SE, Wu MF, Nagpal P, Reed JW (2009) A gain-of-function mutation in IAA18 alters Arabidopsis embryonic apical patterning. Development 136: 1509–1517
Pubmed: Author and Title
Google Scholar: Author Only Title Only Author and Title

Prasad K, Grigg SP, Barkoulas M, Yadav RK, Sanchez-Perez GF, Pinon V, Blilou I, Hofhuis H, Dhonukshe P, Galinha C, Mähönen AP, Muller WH, Raman S, Verkleij AJ, Snel B, Reddy GV, Tsiantis M, Scheres B (2011) Arabidopsis PLETHORA transcription factors control phyllotaxis. Current biol21: 1123-1128
Pubmed: Author and Title
Google Scholar: Author Only Title Only Author and Title

Rao-Naik C, Chandler JS, McArdle B, Callis J (2000) Ubiquitin-specific proteases from Arabidopsis thaliana: Cloning of AtUBP5 and analysis of substrate specificity of AtUBP3, AtUBP4, and AtUBP5 using Escherichia coliin vivo and in vitro assays. Arch Biochem Biophys 379: 198–208
Pubmed: Author and Title
Google Scholar: Author Only Title Only Author and Title

Reed JW (2001) Roles and activities of Aux/IAA proteins in Arabidopsis. Trends Plant Sci 6: 420–425
Pubmed: Author and Title
Google Scholar: Author Only Title Only Author and Title

Ruegger M, Dewey E, Gray WM, Hobbie L, Turner J, Estelle M (1998) The TIR1 protein of Arabidopsis functions in auxin response and is related to human SKP2 and yeast Grr1p. Genes Dev 12: 198–207
Pubmed: Author and Title
Google Scholar: Author Only Title Only Author and Title

Sabatini S, Beis D, Wolkenfelt H, Murfett J, Guilfoyle T, Malamy J, Benfey P, Leyser O, Bechtold N, Weisbeek P, Scheres B (1999) An auxin-dependent distal organizer of pattern and polarity in the Arabidopsis root. Cell 99: 463-472
Pubmed: Author and Title
Google Scholar: Author Only Title Only Author and Title

Scheres B, Wolkenfelt H, Willemsen V, Terlouw M, Lawson E, Dean C, Weisbeek P (1994)

Embryonic origin of the Arabidopsis primary root and root meristem initials. Development 120: 2475-2487

Schruff MC, Spielman M, Tiwari S, Adams S, Fenby N, Scott RJ (2005) The AUXIN RESPONSE FACTOR

2 gene of Arabidopsis links auxin signalling, cell division, and the size of seeds and other organs. Development 133: 251-261

Schlereth A, Möller B, Liu W, Kientz M, Flipse J, Rademacher EH, Schmid M, Jürgens G, Weijers D (2010) MONOPTEROS controls embryonic root initiation by regulating a mobile transcription factor. Nature 464: 913–916
Pubmed: Author and Title
Google Scholar: Author Only Title Only Author and Title

Sieburth LE (1999) Auxin is required for leaf vein pattern in Arabidopsis. Plant Physiol 121: 1179–90
Pubmed: Author and Title
Google Scholar: Author Only Title Only Author and Title

Sridhar VV, Kapoor A, Zhang K, Zhu J, Zhou T, Hasegawa PM, Bressan RA, Zhu JK (2007) Control of DNA methylation and heterochromatic silencing by histone H2B deubiquitination. Nature 447: 735-738
Pubmed: Author and Title
Google Scholar: Author Only Title Only Author and Title

Swarup R, Kargul J, Marchant A, Zadik D, Rahman A, Mills R, Yemm A, May S, Williams L, Millner P,

Tsurumi S, Moore I, Napier R, Kerr ID, Bennett MJ (2004) Structure-function analysis of the

presumptive Arabidopsis auxin permease AUX1. Plant Cell 16: 3069–3083

Swarup R, Kramer EM, Perry P, Knox K, Leyser HMO, Haseloff J, Beemster GTS, Bhalerao R, Bennett MJ (2005) Root gravitropism requires lateral root cap and epidermal cells for transport and response to a mobile auxin signal. Nat Cell Biol 7: 1057–1065
Pubmed: Author and Title
Google Scholar: Author Only Title Only Author and Title

ten Hove CA, Lu KJ, Weijers D (2015) Building a plant:cell fate specification in the early Arabidopsis embryo. Development 142: 420-430
Pubmed: Author and Title
Google Scholar: Author Only Title Only Author and Title

Tian Q, Reed JW (1999) Control of auxin-regulated root development by the Arabidopsis thaliana SHY2/IAA3 gene. Development 126: 711–21
Pubmed: Author and Title
Google Scholar: Author Only Title Only Author and Title

Tzafrir I, McElver JA, Liu CM, Yang LJ, Wu JQ, Martinez A, Patton, DA, Meinke DW (2002) Diversity of TITAN functions in Arabidopsis seed development. Plant Physiol 128: 38–51
Pubmed: Author and Title
Google Scholar: Author Only Title Only Author and Title

Uehara T, Okushima Y, Mimura T, Tasaka M, Fukaki H (2008) Domain II mutations in CRANE/IAA18 suppress lateral root formation and affect shoot development in Arabidopsis thaliana. Plant Cell Physiol 49: 1025–1038
Pubmed: Author and Title
Google Scholar: Author Only Title Only Author and Title

Ulmasov T, Murfett J, Hagen G, Guilfoyle TJ (1997) Aux/IAA proteins repress expression of reporter

genes containing natural and highly active synthetic auxin response elements. Plant Cell 9: 1963-1971

Wang F, Deng XW (2011) Plant ubiquitin-proteasome pathway and its role in gibberellin signalling. Cell Res 21: 1286–1294
Pubmed: Author and Title
Google Scholar: Author Only Title Only Author and Title

Weigel D, Glazebrook J (2002) Arabidopsis, A laboratory Manual, Cold Spring Harb. Laboratory Press, New York
Pubmed: Author and Title
Google Scholar: Author Only Title Only Author and Title

Xu Y, Jin W, li N, Zhang W, Liu C, Li C, Li Y (2016) UBIQUITIN-SPECIFIC PROTEASE 14 interacts with ULTRAVIOLET-B INSENSITIVE 4 to regulate endoreduplication and cell and organ growth in Arabidopsis. Plant Cell 28: 1200-1214
Pubmed: Author and Title
Google Scholar: Author Only Title Only Author and Title

Yamaguchi N, Wu MF, Winter CM, Wagner D (2014) LEAFY and polar auxin transport coordinately

regulate Arabidopsis flower development. Plants 3: 251-265

Yan N, Doelling JH, Falbel TG, Durski AM, Vierstra RD (2000)The ubiquitin-specific protease family from Arabidopsis. AtUBP1 and 2 are required for the resistance to the amino acid analog canavanine. Plant Physiol 124: 1828–1843
Pubmed: Author and Title
Google Scholar: Author Only Title Only Author and Title